STUDIES BY MEANS OF SYNCHROTRON RADIATION

by

OMOTOLA AFOLAYAN OLADIPO

A Dissertation presented to

THE FACULTY OF TECHNOLOGY

of

THE VICTORIA UNIVERSITY OF MANCHESTER

in partial fulfilment of the requirements for

the degree of

MASTER OF SCIENCE

Department of Chemistry
University of Manchester Institute of Science & Technology
Manchester, M60 1QD
England

Submitted: October 1984

TO THE FAMILY

CONTENTS

BIOGRAPHICAL NOTE

The author graduated from the Ahmadu Bello University, Zaria, Nigeria in June, 1981.

He assumed the post of Senior Chemistry Master at Government Secondary School, Wukari, Gongola-State, Nigeria, between 1981 and 1982.

He joined Ahmadu Bello University as a graduate assistant in July, 1982. He has been engaged on a full-time course in Advanced Chemical Technology in the Chemistry Department of the University of Manchester Institute of Science and Technology (UMIST), Manchester, since October, 1983, under the supervision (in part) of Dr B. Beagley.

The author is a table-tennis star and an admirer of the game of snooker.

ACKNOWLEDGEMENTS

I am most indebted to my supervisor, Dr B. Beagley, for the help rendered in the experimentation and the writing-up stages. The knowledge and the enthusiasm generated in the process of his discussions are gratefully acknowledged.

Special thanks are due to Drs. Bredan Gahan and R. Pritchard for helpful discussions and for placing at my disposal many urgent requests.

I would also like to express my gratitude to the staff of the Science and Engineering Research Council, Daresbury Laboratory, Warrington, for providing the necessary facilities in the experimentation stage.

My thanks also go to the Ahmadu Bello University, Zaria, Nigeria, for their study fellowship award and for the dissertation grants which led to the success of this work.

Finally, I owe a debt of gratitude to my wife, Funmilola, for her patience, understanding and encouragement.

DECLARATION

The author declares that no portion of the work referred to in this dissertation has been submitted in support of an application for another degree or qualification of this or any other University or other Institution of learning.

Signed 17/10/84

ABSTRACT

Extended X-ray Absorption Fine Structure [EXAFS) has become known in recent years as a technique for studying the environment of specific elements in chemical systems. This has been related to the advent of synchrotron radiation. The significance of the present studies is to find out how to calculate the EXAFS spectra of our samples, otherwise called "model compounds" (standards or calibrants) viz:

potassium bromide - KBr;

manganese(II) ammonium sulphate hexahydrate - MnSOJNH) SO .6H O;

and strontium bromide hexahydrate - $SrBr_2$.6H O;

from the information available to us from their crystal structures. The EXAFS data for the samples were obtained from the Daresbury Synchrotron Radiation Source and analysed via appropriate UMIST computer programmes. We have assumed that the scattering factors from the Daresbury MUFPOT programme as used in our calculations in the EXAFS region beyond - 70 eV are reliable.

The first objective of the work involved carrying out calculations in the EXAFS regime termed "short-range" refinements for convenience.

The second objective investigated the possibility of extending these calculations to the inner region called XANES (X-ray Absorption Near Edge Structure). Although these calculations gave a fit in the EXAFS region, the fit in the inner region was not satisfactory. The final objective was to attempt to modify the scattering factors in the XANES regime and termed "long-range" refinements. The computer programme involved employed curve fitting by Least Squares, and Fourier transformation techniques. The attempts to modify the scattering factors in the XANES region were largely successful and the results obtained from these studies will be of use in refinements determining unknown structures of compounds with similar atoms to those in the present investigation.

CHAPTER 1

INTRODUCTION TO EXAFS

1.1 Historical Background of the Extended X-Ray Absorption Fine Structure (EXAFS)

The discovery of x-rays by Roentgen[1] about eighty-nine years ago led to a great popular and scientific interest in the penetrating characteristic of x-radiation. Soon after the discovery by Friedrich et al[2] in 1912 of the diffraction of x-rays by crystals, Bragg[3] invented the first flat crystal x-ray spectrometer, using an ionization chamber as detector, and started the analysis of x-ray diffraction phenomena.

The first x-ray absorption spectrum was, however, observed by M. de Broglie[4] using film detection. Though no fine structure was observed, these developments led to the absorption spectroscopy.

Soon measurements at the wavelengths of many absorption edges (see 1.3 below) were made.

The first complicated structure was observed by Fricke[5], working with K-edges of compounds of Mg, Fe and Cr and by Hertz[6] for L-edges of Cs to Nd.

Lindh[7] took it up in his studies of absorption edge structure. Improvement of experimental technique by Lindsay et al[8] and Coster et al[9] showed that metals with the same crystal structure had similar fine structure. However, both groups made fundamental mistakes in their effort to explain the mechanism of x-ray quantum absorption.

Concurrently, Kronig[10] began development of a theory involving Bragg scattering of the ejected photoelectrons by nearby atoms. The theory was developed within the framework of Bloch waves[11] and the then current electron diffraction work of Davisson and Germer[12] and Rupp[13].

The theory showed that an electron traversing a lattice array would have permitted and forbidden zones depending on its wavelength and even when the effect was averaged over all directions in the lattice a residual structure was apparent. It was successful in predicting many experimentally observed features of the fine structure and increasing energy separation of the fine structure features with energy from the edge. A somewhat similar theory was later developed by Hayasi[14] involving quasi-stationary standing waves in the neighbourhood of the absorbing atom. However, it was a long-range order theory and could not account, for example, for the fine structure observed in solid/vapour polymorphs studied by Hanawalt[15].

Recognising this, Kronig[16] described a short-range order theory later developed by Peterson[17] who treated the ejected photoelectron as a plane wave and calculated the scattered wave from surrounding atoms using perturbation theory.

Then began a long period of general acceptance of Kronig's long-range order theory for explaining the results of the so-called Kronig structure in solids. However, neither the experimental data nor the agreement with the theory were sufficient to use the effect for a determination of bond distance or structure.

Kostarev[18] used the Kronig-Peterson[19] short-range order (S.R.O) model to extend the short-range order approach to solid materials. Kozlenkov[20] later built upon Kostarev's work with the result of a quite satisfactory theory of fine structure.

Another short-range order theory was presented by Sawada et al[21], who calculated scattering from individual atoms and included a range term to account for inelastic scattering.

Lytle began measurement in 1960 with an initial goal of extending Hanawalt's[22] temperature effect to cryogenic temperatures to sharpen the fine structure. The result was data sufficient to disprove the wrong long-range order theory for the so-called Kronig structure in solids. Thus a simple empirical short-range order model was constructed which reduced the electron resonances within a sphere defined by the first coordination shell. Although this theory ignored all of the physics of electron scattering, it was successful in extracting accurate first neighbour distances from fine structure data[23].

A conscious effort was made to break away from the Kronig theory and Kronig's structure at the International Conference at Delft[24] under the editorship of Professor Prins. Professor Prins insisted upon an accurate acronym, certainly not the obvious x-ray absorption fine structure (XAFS) which could include the near edge structure.

Finally, extended x-ray absorption fine structure (EXAFS) was accepted as accurate and euphonious. Kronig was reported as attending the same Conference[25].

Lytle et al, beginning in 1968, improved measurements and also improved thetheory of EXAFS[26] confirming the short-range nature of the effect.

In 1971 attempts at Fourier inversion[27] of EXAFS data were successful, providing a great improvement in extraction of structure parameters from the data.

Later developments of EXAFS are described in subsequent sections of this dissertation.

1.2 Synchrotron Radiation in EXAFS Studies

The most dramatic development in the history of Extended X-ray Absorption Fine Structure (EXAFS) was the employment of the high intensity x-ray beams available from a synchrotron radiation[28].

Synchrotron radiation arises as the major energy-loss mechanism from electrons travelling in circular motion at relativistic energies around a synchrotron storage ring.

Properties of synchrotron radiation utilised to advantage in EXAFS experiments include the following:

(a) High intensity;

(b) Broad spectral range

(c) Sharply pulsed time structure and tunability of synchrotron radiation offer unique possibilities for studying conformational changes in biological materials on a subnanosecond time scale; (not considered in the present work)

(d) Natural collimation.

The application of the synchrotron radiation in EXAFS studies as applied to this project is explained in Chapter 3.

1.3 The Phenomenon of EXAFS

X-radiation in passing through matter is absorbed. Extended x-ray absorption fine structure (EXAFS) spectroscopy refers to the measurement of the x-ray absorption coefficient μ, as a function of E - Eo, the photon energy, past the absorption edge at Eo.

Figure 1 shows a typical x-ray absorption cross-section and makes a somewhat arbitrary distinction between x-ray absorption near edge structure (XANES) and the extended x-ray absorption fine structure (EXAFS).

The XANES region addresses the problems of multiple scattering and poor scattering factors and can give details of the local symmetry and other structural data once reliable methods of interpretation have been developed.

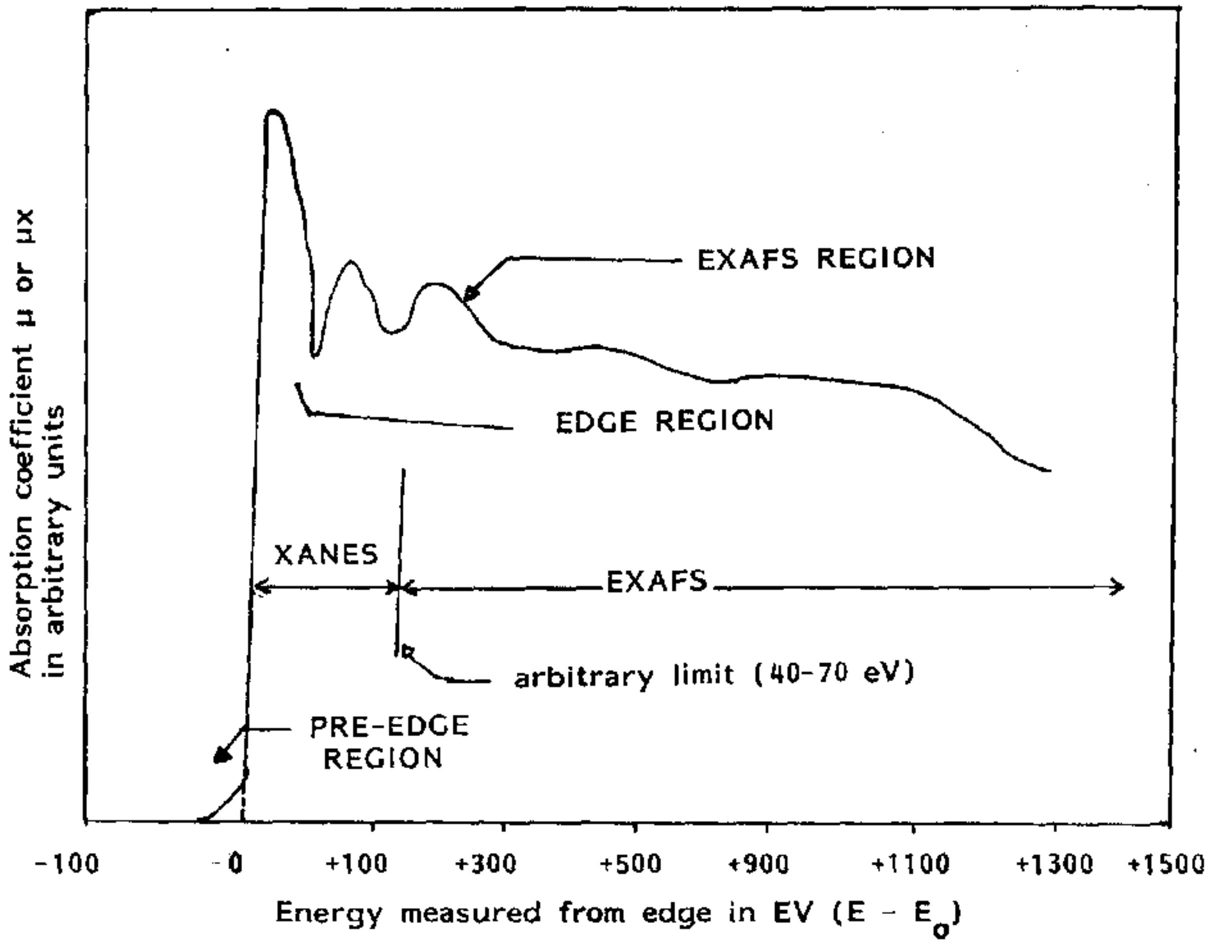

The interpretation of the EXAFS, on the other hand, is much better understood and it is possible to determine radial distance between the central absorber atom and its neighbour atoms, and other parameters. The spectra usually refer to the region 40-1000 eV above the edge.

Normally μ or μx is given by $\mu x = \ln I_o/I$ or $\ln T/T_o$

where μ is the linear absorption coefficient,

x is the absorber thickness

I_o is the incident x-ray intensity

I is the transmitted intensity and T and T_o are the times for a preset count with the absorber in and out of the beam.

Figures 7 and 9 in the subsequent sections show the simple arrangement for obtaining the transmission EXAFS spectrum.

The monochromatic incident x-ray beam has a fixed fraction of its intensity I_o sampled by a detector while another detector measures the intensity I that passes through the sample. Thus $I = I_o \exp(-ux)$.

EXAFS can also be defined as the normalised oscillatory part of μ and is given by $\chi = (\mu - \mu_o)/\mu_o$, where μ_o is the non-oscillatory smoothly varying portion of μ past the edge, i.e. the absorption coefficient of an isolated atom. (Detailed explanation is found in Chapter 2).

Figure 2 conveys the absence of EXAFS in the spectrum of an isolated atom while Figure 3 shows its presence in the case of condensed matter. For isolated atoms, the absorption coefficient decreases monotonically as a function of energy beyond the edge (see Figure 2) but if the absorbing atom is surrounded by a neighbouring atom (as in Figure 3), the outgoing photoelectron wave will be back-scattered by the neighbouring atom, thereby producing an incoming electron wave. The final state is then the sum of the outgoing and all the incoming waves, one per each neighbouring atom. The interference between these oppositely travelling waves gives rise to the sinusoidal variation in absorption coefficient versus energy known as EXAFS.

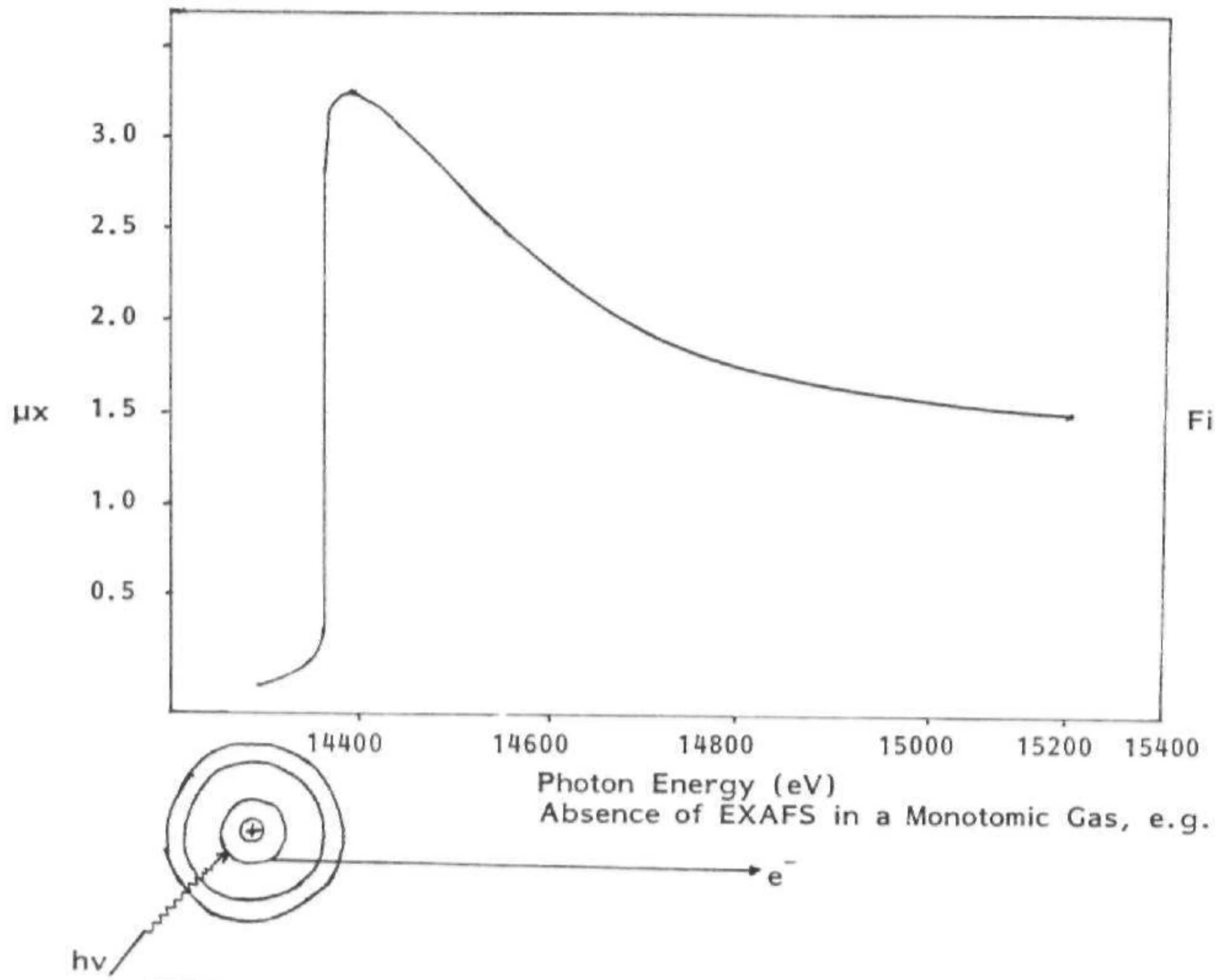

Figure 2

Absence of EXAFS in a Monotomic Gas, e.g. Kr

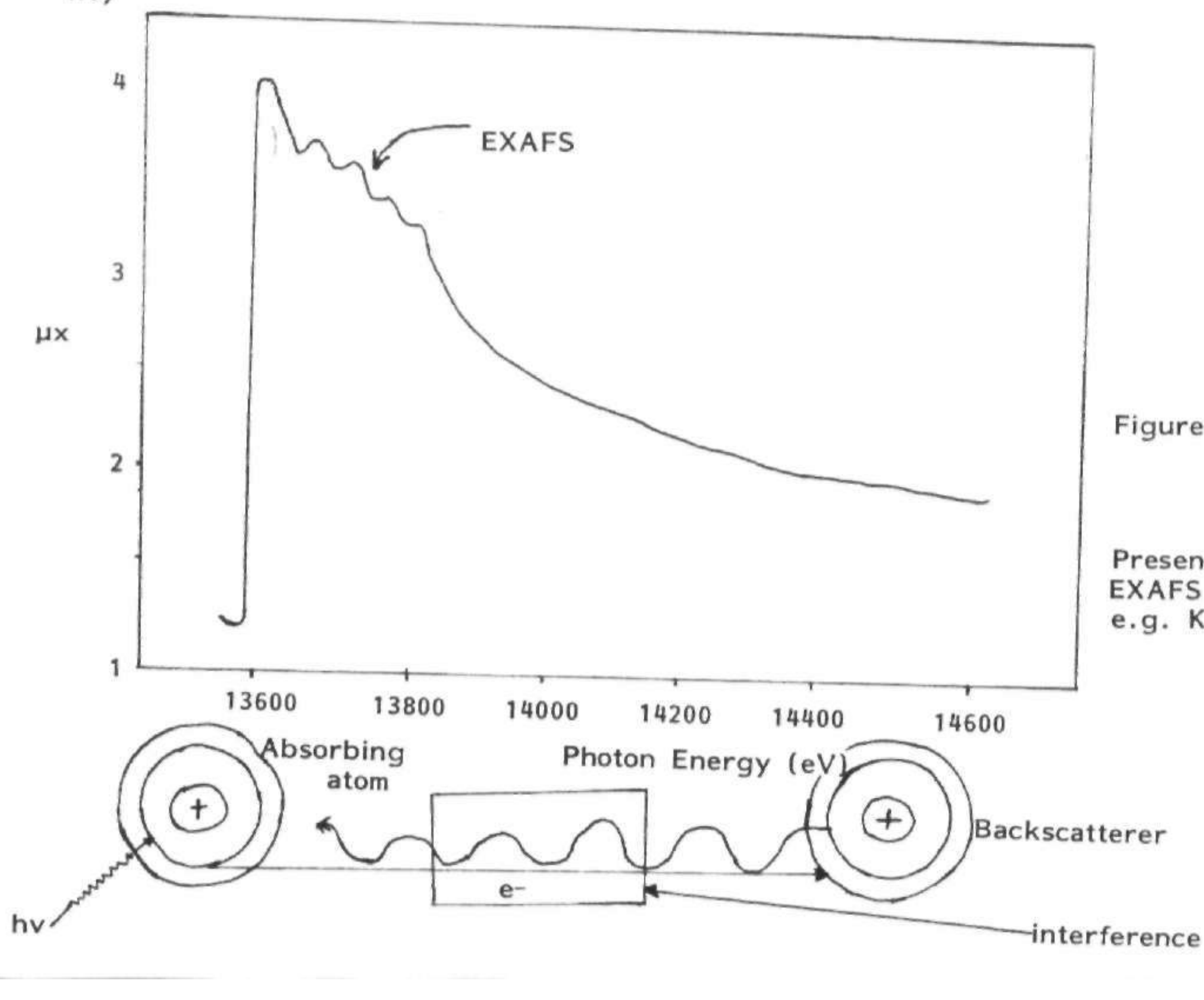

Figure 3

Presence of EXAFS e.g. KBr

The data as plotted in Figure 3 are called raw EXAFS data. The "ripples" give, via computer analysis, quantitative information on the distance between interacting atomic centres, and the numbers of these atoms surrounding the absorber (central atom).

CHAPTER 2

INTRODUCTION TO PRESENT STUDIES

2.1 Proposed EXAFS Studies and Literature Survey

The studies to be described in this dissertation were made at the K-edges of Manganese in manganese(II) ammonium sulphate - $MnSO_4(NH_4)_2SO_4.6H_2O$, and bromine in Potassium bromide - KBr and bromine in Strontium bromide hexahydrate - $SrBr_2.6H_2O$. All the samples were powders.

Besides the advent of Least squares and the Fourier transformation procedures, EXAFS has profited from several recent instrumental and theoretical developments[29]. The EXAFS technique has found good uses in a wide variety of materials such as amorphous solids[30], liquids[31], solutions[32], gases[33], polymers[34] and surfaces[35].

Most work on EXAFS has tended to concentrate on solids or crystalline structure elucidation. The reason is possibly because solids show more rigid structures than solutions or amorphous materials and hence are capable of giving information up to the third neighbouring atoms[36]. On the other hand, crystalline materials can almost always be studied in greater detail by conventional x-ray crystallography[37], which cannot tackle solutions or amorphous materials easily. For this reason, the UMIST group has concentrated its efforts on EXAFS studies of solutions and a brief literature survey, largely of work on solutions, will now be given.

EXAFS studies of dilute solutions have tended to be of first-row transition metals and their compounds[38], because the K-edges of these metals occur at the most easily accessible x-ray wavelengths.

Addressing ourselves more to work of interest to this investigation, Mn–O interatomic distance has been widely investigated by EXAFS technique in solution[39]. The data for $MnBr_2$ and $MnCl_2$ studied in solution gave an Mn–O distance equal 2.200 Å[40]. Additionally, Beagley et al[41], studied EXAFS of aqueous $MnBr_2$ solution and concluded that the complex possesses Mn–Br and Mn–O bonds in solution. The structures of $MnBr_2.4H_2O$ and $MnBr_2.2H_2O$ have been studied and are known[42].

EXAFS data have also been collected by the UMIST group from powdered $MnX_2.4H_2O$ and anhydrous MnX_2 (X = Br, Cl) and a wide range of related complexes, but the computational phase of the work is not complete[43].

M.Y. Ampte and C. Mande[44] also studied Mn-K edge x-ray absorption in its oxides. Rable, Tolkiehn and Werner[45] investigated the K-edge absorption of MnO_2 which they confirmed to have rutile structure with Mn being six fold coordinated.

P. Rabe, G. Tolkiehn et al[46] studied high accuracy bond lengths from EXAFS of solid $KMnO_4$ and MnO_4^- in aqueous solution. The discontinuity of the Mn K-edge in its oxides has been widely investigated by EXAFS technique[47].

E.D. Crozier et al[48] recently carried out EXAFS studies of bromo manganate ions in molten salts.

Closely related to Manganese is Nickel, which also has six water molecules coordinated to the metal in the double ammonium sulphate belonging to the class called the Tutton's salts. Recent work using EXAFS include also $Ni^{(2+)}$ co-ordination in aqueous solution[49]. Results showed, as assumed, $[Ni(H_2O)_6]^{2+}$, i.e. six water molecules were present at 2.04 Å from the metal ion.

As a standard for Br-Br contributions to the EXAFS, Br_2 gas was studied[50]. The Br-Br distance was found to be 2.28 Å, about 0.03 Å greater than the vapour value.

Bromine species have been extensively investigated in polymeric compounds[51]. They are particularly suited for EXAFS studies since bromine K-edge is easily accessible. The same advantage has been utilised in the present investigation. Further, the amplitude of EXAFS in bromine molecules have also been investigated by Stern, E.A. et al[52].

A comparison between the calculated and the experimental spectra of K and Cl in their K-edges studies showed that distant co-ordination spheres are important up to 30 eV above the edge[53].

Other works carried out in EXAFS studies include those undertaken on copper solutions[54], on Zinc and Strontium[55] and on Zinc Chloride solutions[56]. The uniqueness of EXAFS technique in structure investigation has been confirmed by T.M. Hayes[57] in his EXAFS studies of disordered solids and later by V.L. Sukhorukov et al[58] in their fine structure of x-ray absorption spectra of ionic crystals.

2.2 Objectives of Present Studies

The EXAFS data were obtained in experiments carried out at the Daresbury Synchrotron Radiation Source, Warrington. The data for each of the samples were analysed via appropriate UMIST computer programmes. The three materials selected for investigation, viz. Potassium bromide - KBr

Strontium bromide hexahydrate - $SrBr_2.6H_2O$

and Manganese(II) ammonium sulphate hexahydrate - $MnSO_4(NH_4)_2SO_4.6H_2O$ were chosen as "model compounds" (standards or calibrants), whose study would provide vital information to aid more advanced studies. The methods of extracting structural data from EXAFS spectra are still under development and the study of "model compounds" of known structure will remain a vital part of EXAFS investigations of unknown structures for some time to come.

Thus the over-riding aim of the present work is to find out how to calculate the EXAFS spectra of the three materials from the information available in the literature on their crystal structures. The principal obstacle to be overcome is the lack of reliable back-scattering factors (amplitudes and phases) and absorber phases for the near edge (XANES) region of the experimental data. To make progress, we shall make the assumption that the scattering factors obtained from calculations (with the MUFPOT program) carried out at Daresbury, are reliable in the EXAFS region beyond 40-70 eV from the edge.

Proceeding on the basis of the above assumptions, the first objective of the present work is to carry out calculations using only the outer (EXAFS) part of the data beyond ~70 eV. In these "short-range refinements" the need is to obtain a good fit between the experimental (observed) and the calculated (theory) EXAFS curves using the scattering factors available.

The second objective is to investigate whether or not the results from the short-range refinements can be applied to give a fit in the inner (XANES) region also.

The third and the final objective combines the first and the second objecties in an attempt to find a fit for the full range of data, by modifying the scattering factors (if necessary) for the inner region ("long-range refinements").

As mentioned earlier, computer programmes written in Fortran language have been provided for carrying out the objectives. The computer programme used for the third objective has extra functions in the EXAFS equation employed. These then correct the scattering factors in the low energy portion of the curves and improve the fit near the absorption edge.

Refinement is accomplished by means of iterative least squares procedures. It is important to state here that the goodness of fit has been measured by our visual judgement of the fit between observed and calculated spectra as seen on line-printer plots, as well as by consideration of the quantity called the residual, given after each circle of refinement.

The residual is defined as the measure of the similarity of the theoretical (model) and the experimental results.

$$R = 100 \times \frac{\Sigma|\Delta|}{\Sigma|\chi_{obs}|} \text{ per cent}$$

where $\Delta = \chi_{obs} - \chi_{cal}$.

The lower the value of R the better the fit.

It is our aim to retain in the calculations the literature values of interatomic distances extracted from x-ray crystallography studies for each of the compounds. Any correction factors required to obtain a fit with experiments will be refined. The results will be available for use in refinements determining unknown structures of compounds having atoms similar to those in the present studies.

2.3 Current X-Ray Results for the Compounds

In this section, a literature survey of work on the crystal structures of the selected compounds will be given, the structures will be described briefly and the numerical results required for the EXAFS calculations will be given.

The crystal structure of Manganese(II) ammonium sulphate hexahydrate - $MnSO_4(NH_4)_2SO_4.6H_2O$ has been determined by a threedimensional x-ray analysis with Fe $K\alpha$ radiation[59]. The crystals are monoclinic with 2 molecules per unit cell. The six water molecules are arranged about the manganese ion in almost regular octahedron, the average metal-oxygen distance being 2.18 Å[60].

These Mn-O distances show the same pattern as in the other Tutton salts; two pairs of equatorial bonds of 2.18 and 2.20 Å and a shorter pair of axial bonds of 2.15 Å. These are in agreement with previously recorded Mn-O bond lengths in $MnCl_2.4H_2O$[61], although the latter has an octahedron of $4H_2O$ and 2Cl around Mn.

The hydrogen bond network is essentially identical with that found in the other Tutton's salts, that is, each water molecule forms two hydrogen bonds which range in length from 2.72 to 2.86 Å.

Ammonium ions are hydrogen bonded to the oxygen atoms of the sulphate group.

Herrmann opened an era of researches into the structures of $MX_2.6H_2O$ compounds including strontium bromide hexahydrate[62].

Jensen[63] took up from Herrmann in 1940 in further investigation of the function of water of crystallization in hydrates of metallic salts which do not form "coordination compounds".

Strontium bromide hexahydrate's structure was described as being monotonic, with one strontium bromide hexahydrate per unit cell.

The structure of $SrCl_2.6H_2O$ was described in detail by Jensen[64] as it is typical of the trigonal hexahydrates of alkali earth halides. The Sr-O interatomic distances in the chloride were established as 2.62 and 2.80 Å (i.e. $Sr\text{-}O_{(1)}$ = 2.62, $Sr\text{-}O_{(2)}$ = 2.80 Å)

For the EXAFS study of the bromide which was at the Br K-edge, the Br....X distances are required (X = O, Br, Sr). For the chloride Jensen gives Cl....O distances ranging from 3.11-3.57 Å with a mean of 3.28 Å. The shortest Cl....Cl is 4.12 Å.

In the bromide the corresponding distances will be longer; as the EXAFS data is very noisy, it is likely that only the mean Br....O distance will be required. To estimate the lengthening on going from Cl....O to Br....O, the increases in the a and c cell parameters of the trigonal unit cell may be considered.

Parameter 'a' changes from 7.956 to 8.221 Å (3.3%) from chloride to bromide, while 'c' changes from 4.116 to 4.154 Å (0.9%). If a 2% lengthening on going from Cl....O to Br....O is applied, a Br....O distance of 3.35 Å is estimated and this will be used in the EXAFS calculations.

There are two kinds of oxygen atoms in the $MX_2.6H_2O$ structure corresponding roughly in environments to the two types of water molecules proposed by Bernal and Fowler[65]. $O_{(1)}$ is tetrahedral and $O_{(2)}$ is of planar type. Figure 4 shows the suggested structure, which establishes that Sr has 9 oxygen neighbours. Two sets of

3 $O_{(2)}$ are shared with 2 Sr in the column (Figure 4); $O_{(1)}$ is not shared. Le Claire and Bonel (1977)[66] report the structures of $CaCl_2.6H_2O$ and $CaBr_2.6H_2O$ as isostructural with $SrCl_2.6H_2O$, giving Jensen's early study modern support.

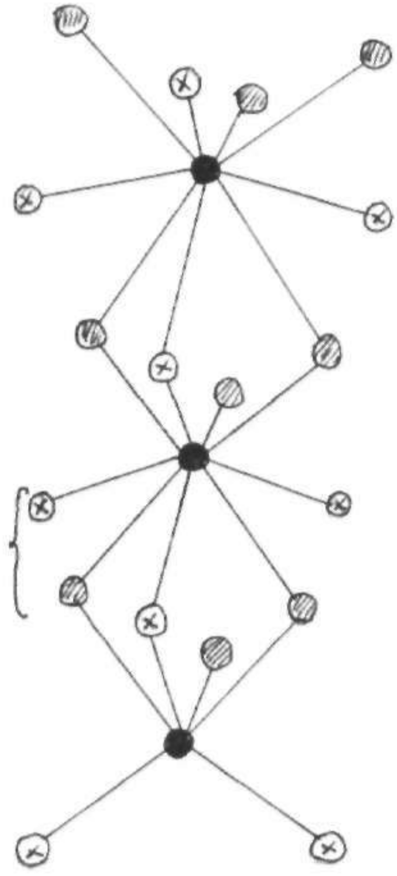

Two types of oxygen atoms suggested

Figure 4 $Sr\text{-}H_2O$ column reported by Jensen for $SrCl_2\text{-}6H_2O$

The thermal parameters of KBr have been studied by several workers using x-ray diffraction[67]. Measurements using powder as well as single crystals have been made. Also, there is considerable disagreement between different experimentalists on the values of the thermal parameters even at room temperature. However, KBr has ben confirmed as having its stable modification with NaCl structure[68].

Potassium bromide has the NaCl, rocksalt, structure, with a cubic unit cell having a = 6.5982 Å[69], with four molecules in the unit cell. The EXAFS calculations may require the distances Br-K (first neighbour) = $\frac{1}{2}$ a = 3.299 Å, next neighbour Br....Br = $a\sqrt{2}/2$ = 4.666 Å and third neighbour Br....K = $a\sqrt{3}/2$ = 5.714 Å. Further distances are readily available if required.

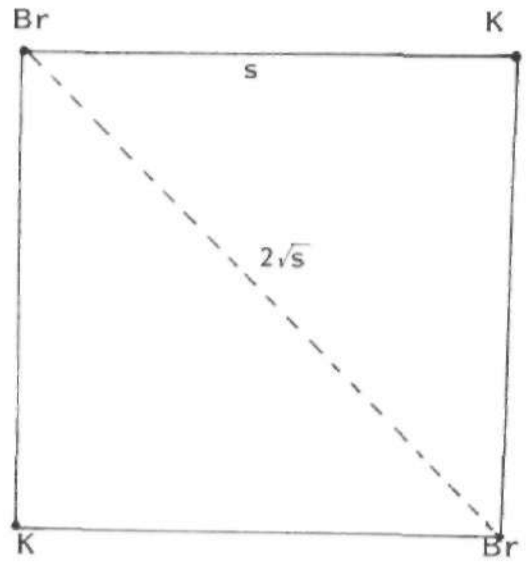

Figure 5(a) A side view of the structure suggested for KBr

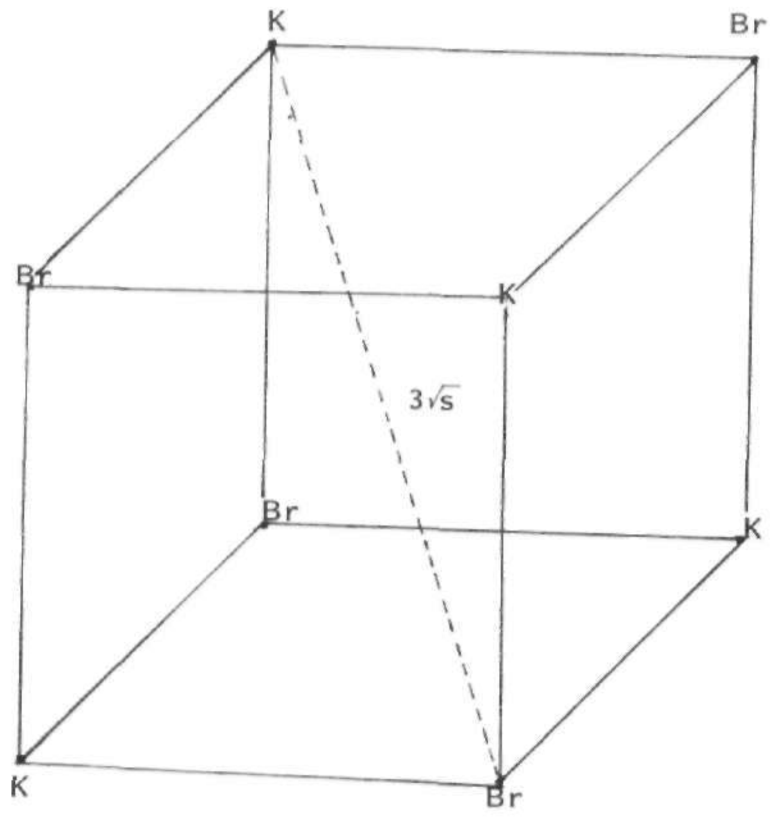

Figure 5(b) A molecule of KBr

Other possible interatomic distances beside K-Br's are masked by dotted lines in Figure (a) & (b)

CHAPTER 3

THEORY OF EXAFS

3.1 Theoretical Aspect of EXAFS

This phenomenon (EXAFS) has been known for half a century as stated earlier in its background history. The basic physical explanation for the theory has been provided by Kronig[70] as being due to modification of the final state of the photoelectron by the backscatterers. Recent work has established the adequacy of a single scattering short-range order (S.R.O) theory, particularly beyond 40-70 eV beyond the edge[71].

The oscillatory part of the absorption coefficient $\Delta\chi$ normalised to the background χ_o is given by[72]:

$$\frac{\Delta\chi}{\chi_o} = -\sum_i 3(\hat{\varepsilon}.\hat{r}_i)^2 \ F(k) \ \sin \frac{(2kr_i + 2\delta_i(k) + \theta(k)}{kr_i^2} \exp^{(-2\sigma_i^2 k^2 - 2r_i/\lambda)}$$

for excitation of an s state in a system by x-ray polarized in the $\hat{\varepsilon}$ direction.

For powders, this equation reduces to

$$\chi(k) = -\sum_i \frac{SF(k)}{kr_i^2} \sin(2kr_i + 2\delta_1'(k) + \theta_i(k)) \exp(-2\sigma_i^2 k^2 - 2r_i/\lambda) \tag{1}$$

Equation (1) describes the modification of the electron wave function at the origin due to the scattering by N_i neighbours located at a radial distance r_i away. S = attentuation factor or the amplitude reduction factor due to many-body effects at the central atom.

The back-scattering amplitude F(k) and phase $\theta(k)$ are given by:

$$f(\pi) \equiv F(k)e^{i\theta(k)}$$
$$= \frac{1}{2_i k} \sum_l (2l + 1)(e^{2_i \delta l} - 1)(-1)^l$$

where δl are the partial-wave phase shifts deduced from wave mechanics and available in tabular form at various levels of approximation.

The electron wave vector k is defined as:

$$k = 2m/\hbar^2(h\nu - E_o)^{\frac{1}{2}} \qquad (2)$$

where $\hbar = \frac{h}{2\pi}$

ν = x-ray frequency

E_o = threshold energy (depends on choice) of the edge

$2kr_i + \theta(k)$ arises due to the phase shifting of the electron wave returning to the neighbour at a distance r_i.

There is also a phase shift of the outgoing electron at the absorber atom δ'_1 (the prime denotes the fact that the central atom is in general different from the neighbour), '1' denotes the value of l, (l = 1). The wave function at the origin is modulated[73]; hence the sinusoidal term in equation (1).

One must account for the fact that atoms are not stationary, as thermal vibration will smear out the EXAFS[74]. This is accounted for in equation (1) by a Debye-Waller type term $\exp(-2\sigma_i^2 k^2)$.

The term $\exp(-2r_i/\lambda)$ where λ is the electron mean free path, accounted for inelastic losses by electrons, though rather crudely[75].

It is the limited range of the photoelectrons in the energy region of interest (50-1000 eV) that permits a short-range order description of EXAFS in materials[76].

Key features of concern in the last few years include the following aspects:

(i) Consideration whether the simple formula given by equation (1) is adequate;

(ii) How to perform the ab initio calculation of the functions $F(k)$, $\delta_1(k)$ and $\theta(k)$ as contained in equation (1) for atoms throughout the periodic table and test them against experiments.

This second aspect has been dealt with by Teo et al[77] based on the theoretical developments of Lee and Beni[78].

Finally, it was established that if the E_0 (threshold energy) is allowed to vary as an adjustable parameter, the calculated phase shifts are in good agreement with experiments[79], thus enabling nearest neighbour distances to be determined with an accuracy of ca 0.02 A.

It is now generally accepted that much of the inadequacy of equation (1) is due to multiple scattering, which has its greatest effect in the XANES region This and other sources of inadequacy will now be discussed.

(i) Multiple Scattering

Equation (1) takes into account only a single back-scattering. It is a fact that EXAFS is an interference phenomenon and obviously related to Low Energy Electron Diffraction (LEED) and angular resolved photoemission[80]. In short, EXAFS can be likened to LEED with a source and a detector located in the absorber[81].

The fact that multiple scattering is known to be very important in LEED makes single scattering formula inadequate in equation (1).

The clue to this problem is that one can account for multiple scattering events using equation (1) by adding all scattering paths that originate and terminate at the absorber (see figure 6).

Each of these events behaves like $\sin(2kr_{eff})$[82] where $2r_{eff} = r_1 + r_2 + r_3$ is the total path length. Thus multiple scattering events give rise to rapidly oscillatory contributions in k space, and are particularly important for backscatterers beyond the first neighbours of the absorbing atom These distant backscatterers contribute more in the XANES than in the EXAFS regions[83].

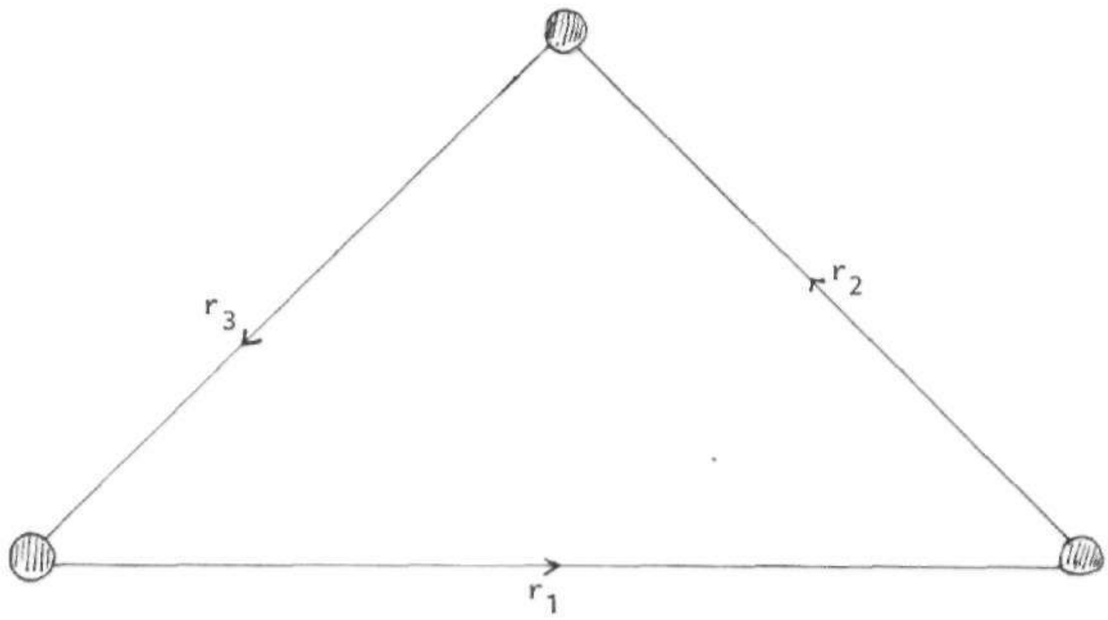

Figure 6 Illustration of a multiple scattering event.
$2r_{eff} = r_1 + r_2 + r_3$ (r_{eff} = effective path length)

(ii) Chemical Transferability of Phases

Effects such as chemical bonding, non-spherical potential, atomic configuration and ionicity have a decreasing influence on the phase shift functions for increasing energy[84]. Such effects are ignored by equation (1); otherwise, E_o can change to mimic them. This is the basis of the calculated phase shifts used in bond-length predictions. This has been found experimentally for a limited number of cases in the early years of development of EXAFS as a tool for investigating structure by Stern et al[85], Lytle et al[86]. A later, more detailed study on EXAFS theory by Citrin et al[87], Patrick Lee[88] further confirmed an approximate compensation of these effects by varying E_o.

Amplitude and phase transferability:

Equation (1) modelled inelastic losses by an exponential damping term $\exp(-2r_i/\lambda)$. This has been found to be inadequate. A confirmed discrepancy between the calculated amplitude and the experiment has been found to be due to the core hole relaxation processes[89] in the central atom. Many investigations have been carried out to confirm this, the best documented case being that of Br in Br_2 molecule by Stern et al[90], 1979, and later of CuBr solid by Stern et al[91], 1980.

(iii) Thermal and Static disorder

Equation (1) assumes that disorder can be accounted for by a Debye-Waller type factor $\exp(-2\sigma^2k^2)$. This term assumes that the disorder is harmonic in the case of thermal disorder. Systems with large thermal disorder, e.g. Zn at high temperature[92], super-ionic conductors of large intrinsic disorders are exceptions[93]. Other "disorder" like cases where the absorber occurs in a variety of environments in the sample, is also important[94].

The effect of "disorder" tends to reduce the EXAFS amplitude rather as a Debye-Waller factor. This can affect measurements of the number of nearest neighbours. It is confirmed that deviation from Gaussian behaviour produces phase shift corrections[95].

An expression for σ as a function of temperature was first given by Schmidt[96,97] based on the debye approximation for lattice vibrations. This was later re-derived and somewhat generalised to include anisotropy by Beni and Platzman[98]. Going beyond the

Debye approximation the exact expression for σ in the harmonic approximation was numerically calculated for several force constant models of Cu, Fe and Pt by Sevillano et al[99]. Rehr[100] simplified this in 1979 to include amorphous solids. Further investigations were recently carried out in this area by Rehr[101], Rabe et al[101], Böhmer and Rabe[103] and Eisenberger and Brown[104].

CHAPTER 4

EXPERIMENTATION

Most recent EXAFS work is done using synchrotron radiation. The growth of EXAFS has been closely tied to that of synchrotron radiation sources because of the need for an intense, broadband source of x-radiation.

Synchrotron radiation is emitted when relativistic charged particles travel in curved paths in magnetic fields. Hence it arises as the major loss mechanism from electrons in circular motion.

4.1 The Equipment

There are several well-developed modes of EXAFS measurements most of which use photons as the primary source of excitation. We shall, however, be concerned with transmission mode of the EXAFS spectrometer as shown below in Figure 7.

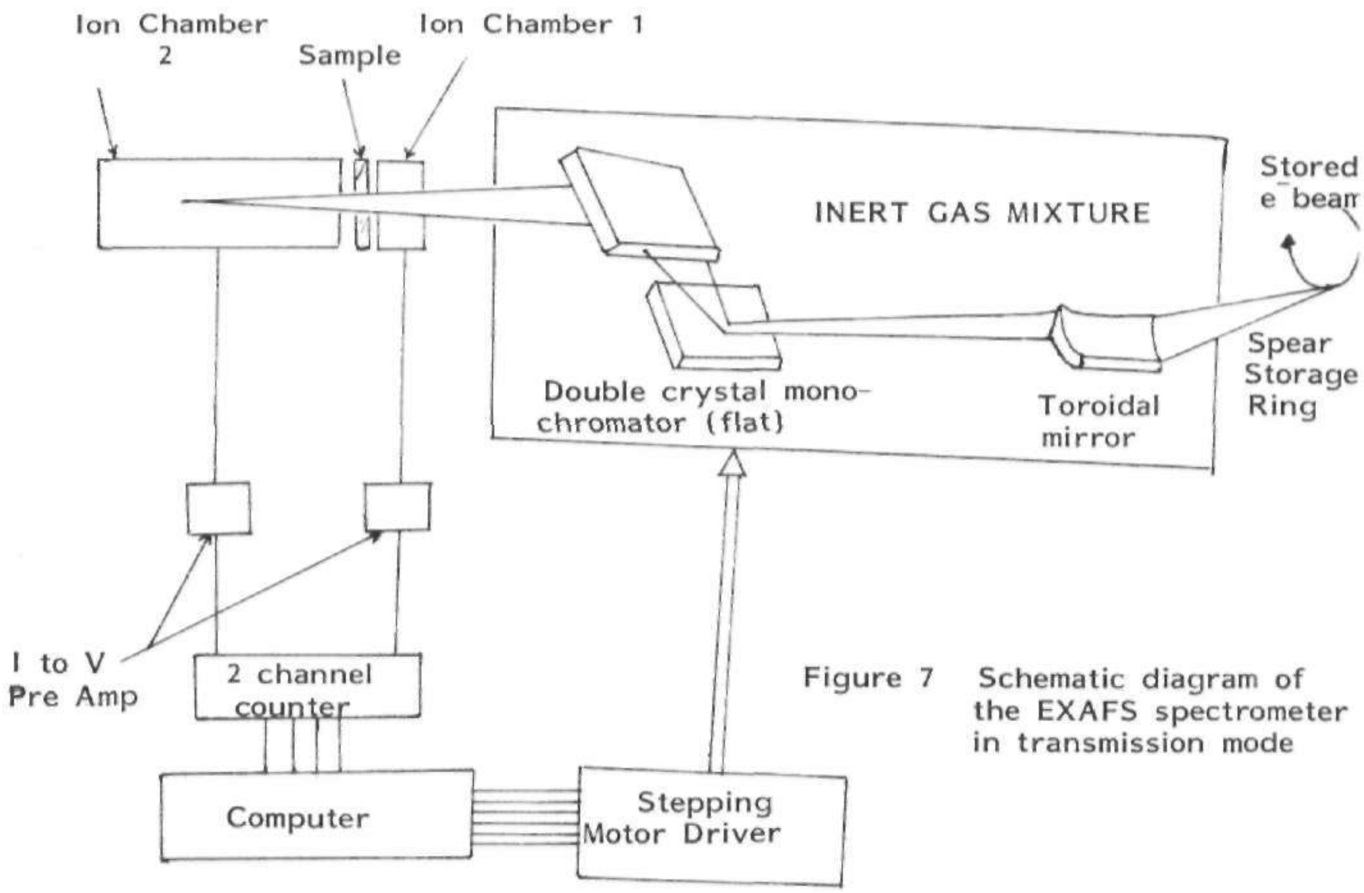

Figure 7 Schematic diagram of the EXAFS spectrometer in transmission mode

The synchrotron radiation from the electron storage ring represented by a broken cycle at the upper right corner, is collected by a toroidal mirror and monochromatized by a double crystal monochromator. Alternatively, the radiation can be monochromatized with a curved mirror monochromator. The chamber is filled with rare gas mixtures to suit the spectra wavelength range chosen.

The configuration of a channel-cut crystal or a parallel double-crystal monochromator is shown in Figure 8.

For a selected Bragg spacing d, the central wavelength, λ, of the output beam will be

$$\lambda = 2d_{hkl}\sin\theta_B$$

When the input beam makes an angle θ_B with the Bragg planes (i.e. satisfying the Bragg reflection condition), the output beam is displaced from the input beam by $h = 2D\cos\theta_B$ where D is the spacing - usually 1 cm, between the two crystals and θ_B is the Bragg angle for the chosen reflection. The arrangement ensures that the output and the input beams propagate in the same direction. Furthermore, the position of the sample in the beam can be maintained by the small vertical translation h.

The incident beam intensity is measured by the ionization chamber 1 and the transmitted beam intensity by the ionization chamber 2 (see Figure 7).

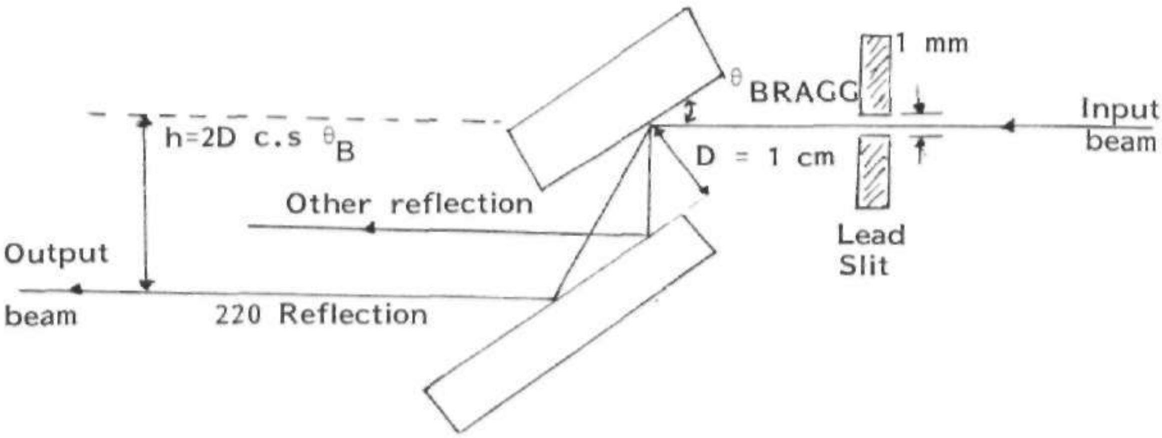

Figure 8 Schematic diagram of a channel cut crystal monochromator

The energy of the beam is changed by changing the angle between the monochromator crystal and the incident beam. Figure 9 shows a general layout.

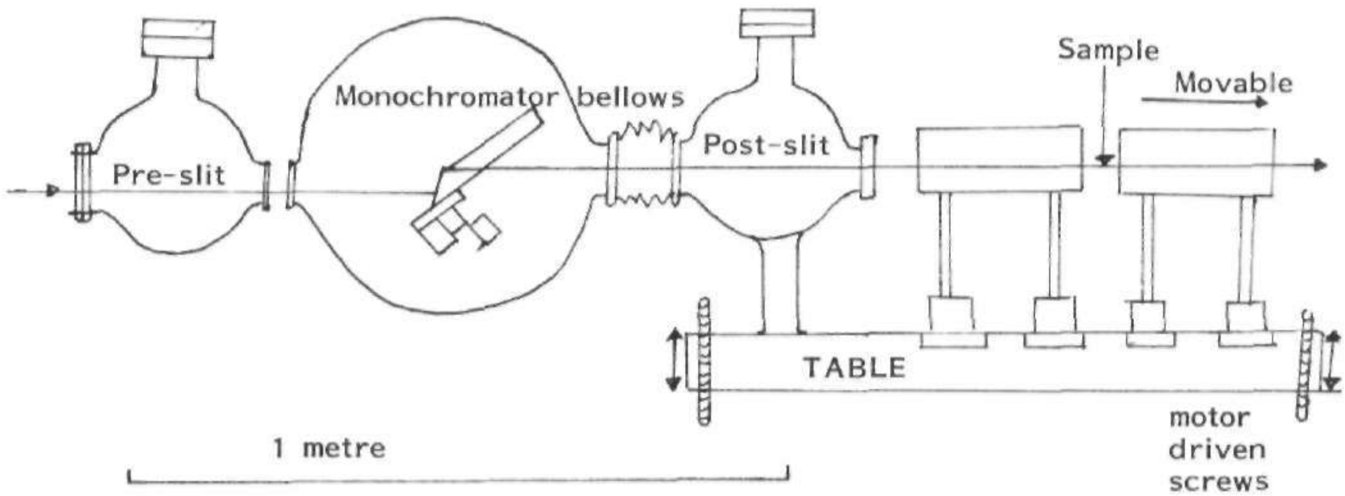

Figure 9 Experimental arrangement for measuring EXAFS in transmission mode

The synchrotron source used in this investigation was at the Science and Engineering Research Council's Synchrotron Laboratory at Daresbury, Warrington.

The beam line 7 EXAFS station 7.1 is situated 16.5 metres from the storage ring tangent point and may be used with the focused or non-focused optics. Detector, exit slits and sample chamber are mounted on a stepping-motor-driven table as in Figure 9.

The table follows under computer control the parallel shift of the monochromatic beam as the monochromator crystal is rotated. Channel cut Si(111) or Si(220) crystals monochromators are used.

All the equipment shown in Figure 9 is situated inside a radiation hutch fitted with interlocking safety equipment to cut off the beam in any unsafe situation.

The step motors which rotate the monochromator, move the slits and table, are controlled by an $LSI/11/O_2$ computer which also accumulates the data and stores it on floppy disks.

The data so stored are transferred to the main frame via a data concentration onto a magnetic disk for final transfer into files in the University of Manchester Regional Computer Centre (UMRCC).

4.2 Preparation of Samples

The absorbing samples were prepared by grinding to pass 400 mesh and sandwiched between strips of sellotape for support and thermal contact and attached to the sample holder. This represents the sample cell.

(ii) Experimental Procedure

The sample cell is positioned in the path of the x-radiation beam on EXAFS line 7 at Daresbury.[105]

A standby laser beam set to coincide with the x-ray beam may be used to align the sample cell well in the path of x-radiation. When the hutch door was securely fastened and all safety procedures satisfactorily observed, the scans were carried out. Suitable wavelength range was selected to scan through the absorption edge for a sample. A silicon (111) monochromator crystal was used.

For the $MnSO_4(NH_4)_2SO_4.6H_2O$ complex, for example, the Manganese (absorber) K-edge was known to be at 1.896 Å $\theta = 17.601^\circ$ for Si(111) thus making the λ, range selection easier as in Table 1.

The contents of each region are displayed on the VDU. These scan parameters are for a single scan of two regions starting at 17.8 degrees and ending at 16.5 degrees. The number of steps the monochromator moves before a reading is taken is determined by incr (short for increment). Time is measured in milliseconds and the values for the reference and signal are counts from the ion chambers (see Table 1).

TABLE 1

Region 1		
Start	17800	100,000
Incr.	10	8,000,000
End	17640	80,000
Region 2		
Start	17640	100,000
Incr	2	8,000,000
End	16800	80,000
Region 3		
Start	16800	100,000
Incr	5	8,000,000
End	16500	80,000

With EXAFS equipment (Figure 7) set in transmission mode, the monochromator was moved by varying the Bragg angle, and hence the wavelength ($\lambda = 2d\sin\theta_{Bragg}$), whereupon the full EXAFS spectrum was obtained. More x-rays obviously passed through the sample as angles were decreased, but the count I_o is limited by a constant I. More data points were recorded in the region close to the absorber edge. The whole experiment is performed under the control of the computer situated outside the hutch.

4.3 Data Processing

The first step was to condense the individual I and I_o counts that were collected on each sample into one final coded spectrum.

The data are then expressed as a relative EXAFS modulation, generally defined by[106]:

$$\chi(k) = [\mu(k) - \mu_{BG}(k)]/\mu_o(k) \qquad (2)$$

where χ is the fine structure modulation (EXAFS)

μ is the observed x-ray absorption cross-section

μ_o is the photoelectric cross-section for the free atom

μ_{BG} is the experimentally derived background

In equation (2) the EXAFS modulation χ is not expressed as a function of the incident x-ray photon energy but as a function of the resultant photoelectron wave vector defined by:

$$k = 2\pi(2m_e[E - E_o])^{\frac{1}{2}}/h$$ (also shown in Chapter 3),

where k is the photoelectron wave vector which has units of 1/distance

E is the energy of the incident photon, E_o is the K-shell binding energy,

m is the mass of the electron and

h is Planck's constant.

To obtain $\chi(k)$ from an x-ray spectrum, a number of procedures are utilised.

First, a pre-absorption edge background is removed from the spectrum. Then the spectrum is divided by the free-atom photoelectric cross-

It is often very useful to create simulated data and compare the Fourier transforms and the fitting results with the unknown system, and this is what this study seeks to achieve.

The flow chart (Figure 10) from Cramer et al[108] suitably illustrates a typical complete data processing procedures.

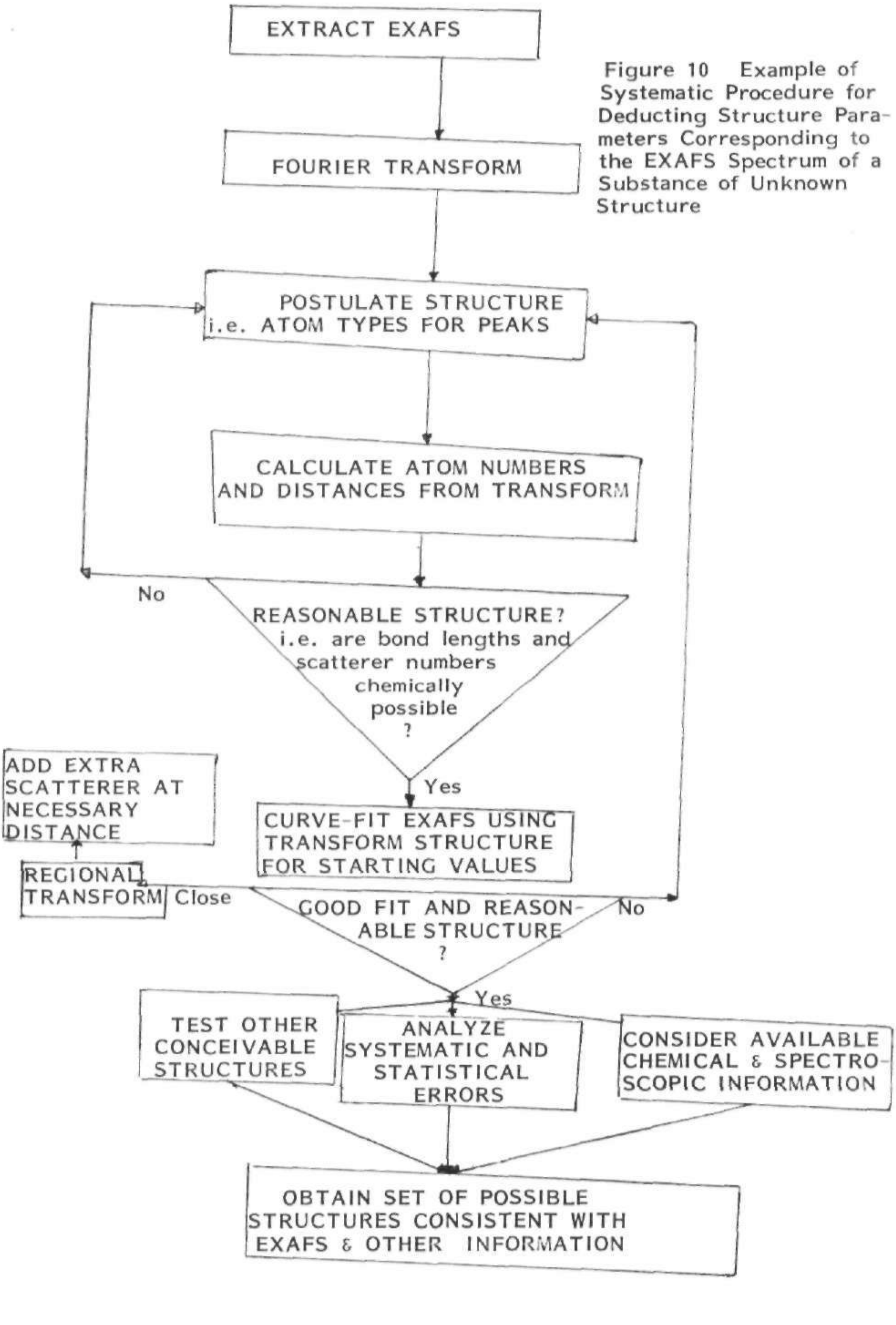

Figure 10 Example of Systematic Procedure for Deducting Structure Parameters Corresponding to the EXAFS Spectrum of a Substance of Unknown Structure

4.4 Analysis of Data (Computing Procedures)

Quantitative treatment of raw EXAFS data is best handled by means of computer programming, for accurate extraction of structural and chemical information.

Computer treatment of the raw EXAFS data normally commences at Daresbury Synchrotron Radiation Laboratory with a programme called EXCALIB. This programme, starting with the experimental data file, produces normalised spectra of absorption versus electron energy in eV and Hatrees.

The next program EXBACK is an interactive programme available for removing background from either absorption or fluorescence excitation spectra.

The final files of EXAFS curves were transferred to the University of Manchester Regional Computer Centre (UMRCC) files for further processing using UMRCC/7600 joint system. This system is linked directly with UMIST terminals, thus enabling easy access via ROSCOE on the AMDAHL computer.

Scattering factors (i.e. amplitudes and phases) assumed to be appropriate, obtained from quantum mechanical calculation (MUFPOT program) at Daresbury, were available in files also containing raw EXAFS data for each of the three compounds. Good scattering factors are required to get a good fit between experimental and the model data.

We have analysed the data using Fourier transform and the curve-fitting computer programs.

Curve fitting involves a best fitting of the data with a sum of individual waves modelled by empirical equation (1), each of which contains appropriate structural parameters for each type of neighbour and the appropriate scattering factors.

On the other hand, the Fourier transform technique provides a photoelectron scattering profile as a function of the radial distance from the absorber, and help to provide starting parameters for the curve fitting.

The problems of the Fourier transform technique include:

1. "side lobes" (due to nonlinear character of the phase and the amplitudes) which can interfere with the weaker peaks and
2. skewing of the transformed envelope (due mainly to structure) which may affect the peak position.

The problems of curve-fitting methods include:

1. multi-dimensional parameterisation which can be very time-consuming; and
2. correlations among various parameters.

In either method, the data used are the $\chi(k)$ vs k curves from the EXBACK programme. $\chi(k)$ can be fitted without modification (our standard method) or multiplied by some power of k so as to compensate for the diminishing amplitudes at high k values to give k^n (k), for which a weighting scheme n = 3 is commonly used.

Additionally, excellent standard computer programs of UMIST are available which make the two techniques quite automatic once the data are provided.

The "model compounds" possess Sr-O distances in $SrBr_2.6H_2O$; Mn-O in $MnSO_4(NH_4)_2SO_4.6H_2O$; and Br-K and Br-Br in KBr.

We have examined each of these interatomic distances present by full-matrix least squares curve fitting calculations based on the original EXAFS χ-curves and refining a number of parameters until a fit was obtained. Sometimes longer (second neighbour) distances were included.

For the EXAFS region of each data we have refined the following parameters:

i. interatomic distance between the absorber and the scatterer represented by variable R_1 in the computer programme (and sometimes R_2 for a second back-scatterer) or ΔR, the correction needed to make the EXAFS data fit the literature distances;

ii. the zero energy correction represented as ZERO;

iii. the vibrational amplitudes U_1 (and U_2) and

iv. we have modified the background treatment for a good fit.

Presence of large number of ripples in the printout have suggested the possibility of other distances other than R_1. In such cases, as observed in KBr and $MnSO_4(NH_4)_2SO_4.6H_2O$; we have included distance R_2 and its multiplicity. The effect of this procedure on the fit is presented under results and discussion.

As for the XANES region, we have kept the parameters already refined in the EXAFS region fixed, and refined only those parameters which modify the scattering factors below an also refinable EXAFS/XANES limit.

In short, we have applied equation (1) in our calculations at K (or E) equal to or greater than the limit value from our assumption that the scattering factors were known in that region (i.e. we have made no correction in the scattering factors beyond and at the limit value) See Figure 11(a).

However, the scattering factors below the limit value (inner region) have to be modified as entailed in the new use function applied for a good lfit in the XANES region. This users function contained modified amplitude and phase functions as:

Amplitude (F(k)):

$$F(k)\ [1 + (\underset{\text{value}}{\text{limit}} - \underset{\text{k or E}}{\text{actual}}) * \text{amplitude adjustment constant}]$$

This modified amplitude function, applicable only if k (or E) is less than the limit value, is represented schematically by the broken line in Figure 11(b). This diagram implies that the correction needed for a satisfactory fit increases the amplitude. This is normally so.

Phase $(= 2\delta' + \psi(k))$ = **PH**:

becomes [PH + (limit − actual) * phase adjustment constant]
value k or E

The diagram Figure 11(c) of the modified phase shows that the correction needed in the inner region for a good fit, reduces or increases the phase. Either reductions or increases may occur.

We hoped the modified scattering factors would improve the fit in the inner regions of the curves. In this technique we have treated the following as adjustable parameters for each back-scatterer;

(i) limit of the EXAFS region with the XANES;

(ii) the Phase Adjustment Constant; and

(iii) the Amplitude Adjustment Constant.

With the above procedures well employed we have hoped for a better fit between an experimental and the theoretical data.

Figure 11

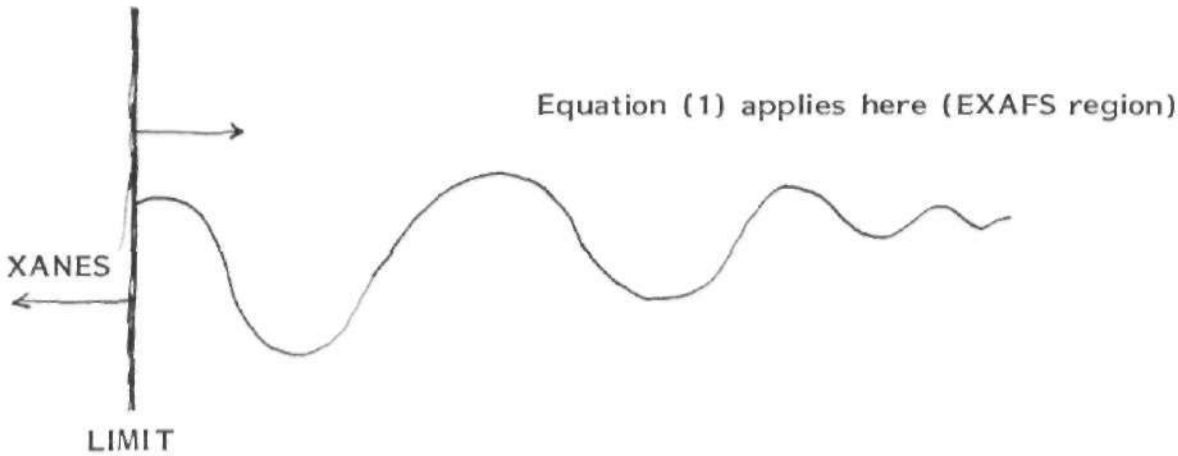

(a) We assume the values supplied by quantum mechanical calculations are correct in the EXAFS region.

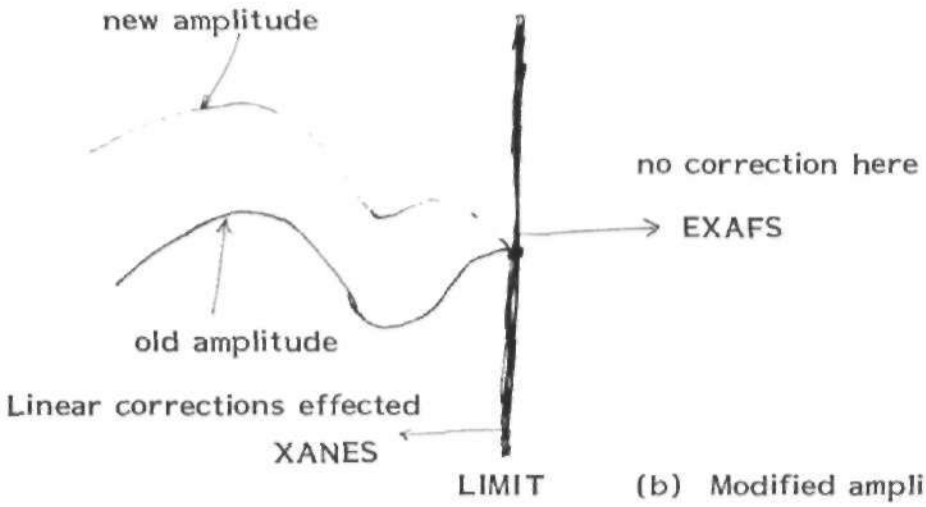

(b) Modified amplitude

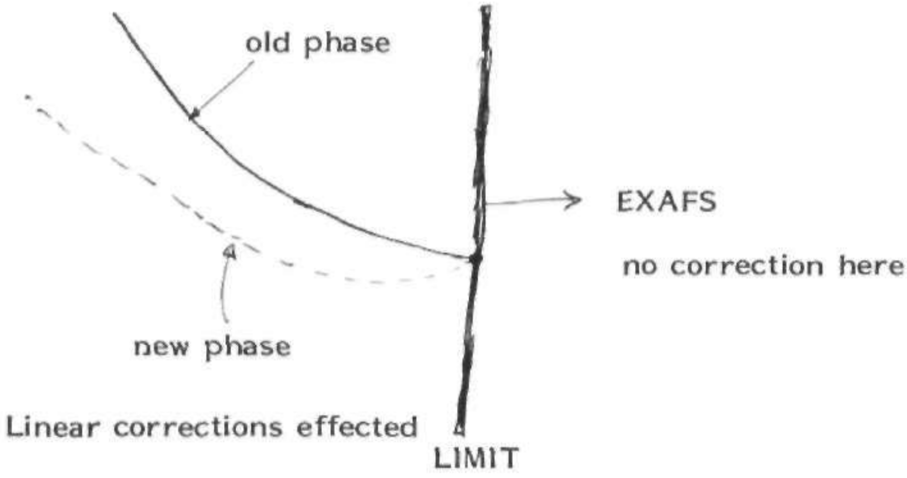

(c) Modified phase.

CHAPTER 5

SUMMARY OF RESULTS

CHAPTER 5

SUMMARY OF RESULTS

5.1 Introduction

Structural parameters extracted from the literature for each compound were used as the initial values in the refinements. The early part of the investigation involved the use of a computer program (Appendix 1) which has no refinable ΔR (DelR, the correction needed to make the EXAFS values fit the literature values) but which possesses $\Delta R = 0.41$ Å in the users function of the program. The results shown in Table 3 were obtained in the preliminary stage of the investigation.

We then employed another computer program which enabled ΔR parameters to be refined with the R'S (interatomic distances) fixed at the literature values. We have used the program to refine these adjustments to the literature values of the distance parameters required to fit the EXAFS data. The program was applied to each of our sets of EXAFS data using both "short-range" and "long-range" methods of refinement. The results of the short-range refinements (EXAFS region) are shown in Table 4. This method was also tried to fit the inner region (XANES) without optimising the scattering factors in that region. Typical results are shown in Table 5 for $MnSO_4(NH_4)_2SO_4.6H_2O$ for example, the high residual shows that the program used in fitting the EXAFS region (E > 2.50 Hatree) gives poor fits for the XANES region unless some modifications are made in the functions employed.

The poorness of the fit is evident from the plot shown in Figure 21. The poor fit is observed throughout the curves with different values being obtained for the refined parameters compared with those in Table 4. It is unlikely that a good fit can ever be achieved without allowing the scattering factors to be adjusted in the XANES region ($E < 2.5$ Hatree). We have used the program described in section 4.4, which permits adjustment of the scattering factors to achieve this. The new users function was then applied which attempted and succeeded in fitting the XANES region of the curves. Refinements carried out with this program adjusted the scattering factors in the inner region to give a good fit between the theoretical and the experimental data. The results of this technique are presented in Table 6, with the estimated standard deviations in brackets. This version maintains the fit fixed from the "short-range" (EXAFS) refinement, thus fitting well throughout the whole range of data.

A full description of the background optimisation and of the structural parameters involved in the refinements will now be given.

BACKGROUND REFINEMENT

This is an important aspect of the investigation. We have employed background instructions supplying a minimum and a maximum energy value defining the required range of data to be included in the refinement; in addition, we choose a suitable background code which controls the smoothness of the new background fitted.

The choice of E_{max} and E_{min} depended on the nature or the experimental range of data of each sample. In $MnSO_4(NH_4)_2SO_4.6H_2O$, for example, E_{max} was extended to 11.95 Hatree after which the data became too noisy.

<u>Zero</u>

Zero is a measure of the zero error of the energy arising from poor choice of edge position during pre-treatment of the raw EXAFS data. Calculations with zero value between 0-0.02 have been found to give better fit in the EXAFS refinements, whereas results from "long-range" refinements without scattering factors modification have been observed to give negative zero values in an attempt to fit the regions. The incompatibility of zero values from these short and long-range refinements reflects the unsatisfactory nature of the unmodified scattering factors. Many jobs were run in the process of correcting these parameters.

<u>R1, R2, R3</u>

These parameters represent the interatomic distances involved in the investigation. Whether to include more than one distance in a refinement depends on the nature of the EXAFS data. A set of data with large number of irregular ripples suggests more than one interatomic distance present, e.g. KBr data. Weak ripples superimposed on the main oscillations suggest hydrogen-bonded water in the case of Mn sample.

MULTIPLICITY

This is represented as MULTR1, MULTR2, etc. in the programs. MULTR1 defines the number of nearest neighbours and is kept fixed. A series of jobs were run until suitable values of other multiplicities were obtained, the variable values arising from multiple scattering effects. We normally refine these parameters only after most other parameters have converged. However, results for these parameters do not represent number of neighbours because of the multiple scattering effects. Thus, large multiplicity values may be acceptable in the EXAFS technique.

MEAN FREE PATH, λ

The mean free path, λ , term allows for contributions from inelastic electron scattering. The λ effect is equivalent to a finite lifetime of the excited state. It measures the average distance an excited electron can travel before losing coherence with its initial state. Refinement of this parameter is particularly important in the "long-range" refinement because the final state electrons have long mean free paths at low energies leading to the emergence of multiple scattering as a significant factor in determining the EXAFS for K less than 2 or 3 $\mathring{A}^{-1}$.

LIMIT, AMPLITUDES AND PHASE ADJUSTMENTS

These parameters are necessarily refined in the final "long-range" refinements, in order to fit the inner region of the EXAFS spectra concerned. While negative or positive value may be admissible for the phase adjustment, a negative value for amplitude adjustment usually accompanies a bad fit. Often the course of the refinement has to be carefully controlled so that it converges to a positive value.

Table 2 lists the variables in their annotated form for KBr data as an example to illustrate parameters used in the refinements but which have not been included in the description.

Card	Variable	Explanation of Variable
V/1	R1	Br-K distance
V/2	$U_1 = U_2$	Vibrational amplitude
V/3	Mult R1	Multiplicity for Br-K distance
V/4	Phase R1	Br-K phase
V/5	FP R1	Free path of Br-K
V/6	FP power 1	Free power of Br-K
V/7	Del R1	Correction to Br-K distance
V/11	R2	Br-Br distance
V/12	U_2	Vibrational amplitude
V/13	MULTR2	Multiplicity of Br-Br
V/21	R3	Br-K distance
V/22	U_3	Vibrational amplitude
V/23	MULTR3	Multiplicity of Br-K
V/27	Del R3	Corrections to Br-K distance
V/41	ZERO	Zero error in energy scale
R/1, R/2, R/3, R/4	These cards indicate the atoms involved in the distances and provide a further way of defining the multiplicities.	

By varying some of these parameters, we have set to obtain a good fit between experimental and the calculated data.

TABLES OF RESULTS

Table 3: Gives results of the refinements of the EXAFS for each of the sample data with program which has no refinable ΔR (but which possesses ΔR = 0.41 Å in the users function) (Early stage of the investigation)

"Model Compound": $MnSO_4(NH_4)_2SO_4.6H_2O$ R = 11.1%

Estimated Standard Deviation (e.s.d.) in brackets

Parameters Refined	Values
R1 (literature value)	2.180 Å
R1 (EXAFS)	2.2457 (22) Å
$U_1 = U_2$	0.099 (1) Å
Zero	0.057 (10) Hartree

Energy Range: 2.50-8.00 Hartree

"Model Compound": $SrBr_2.6H_2O$ R = 23%

Parameters Refined	Values
R1 (literature value)	3.350 Å
R1 (EXAFS)	3.234 (15) Å
$U_1 = U_2$	0.027 (11) Å
Zero	0.087 (30) Hartree

Energy Range: 2.50-5.00 Hartree

"Model Compound": KBr   R = 21%

Parameters Refined	Values
R1 (literature value)	3.299 Å
$U_1 = U_2$	0.192 (2) Å
Zero	0.356 (4) Hartree
R1	2.705 (14) Å

Energy Range: 2.50-5.00 Hartree

Table 4 Gives results of the refinements obtained from a computer program which enabled ΔR parameters to be refined with R's fixed at literature values of each compound.

"Model Compound": $MnSO_4(NH_4)_2SO_4 \cdot 6H_2O$ R = 7.7%

Parameters Refined	Values
R1 (literature value)	2.180 Å
R2 (literature value)	4.314 Å
$U_1 = U_2$	0.1111 (3) Å
DelR1	0.326 (1) Å
Mult R2	7.3 (30)
Zero	0.126 (4) Hartree

Energy Range: 2.50-11.95 Hartree

"Model Compound": $SrBr_2 \cdot 6H_2O$ R = 37%

Parameters Refined	Values
R1 (literature value)	3.350 Å
$U_1 = U_2$	0.113 (3) Å
DelR1	0.276 (9) Å
ZERO	0.148 (23) Hartree

Energy Range: 2.50-8.20 Hartree

"Model Compound": KBr R = 34%

Parameters Refined	Values
R1 (literature value)	3.299 Å
R2 (literature value)	5.714 Å
$U_1 = U_2$	0.142 (2) Å
DelR1	0.471 (3) Å
DelR2	0.242 (11) Å
Zero	0.148 Hartree

Energy Range: 2.50-8.00 Hartree

Table 5: Gives an example of curve-fitting results in XANES region (E < 2.5 Hartree) without modifying scattering factors

"Model Compound": $MnSO_4(NH_4)_2SO_4.6H_2O$ R = 26%

Parameters Refined	Values
R1 (literature value)	2.180 Å
$U_1 = U_2$	0.169 (3) Å
FR P1	0.611 (22) $Å^{-2}$
DelR1	0.399 (7) Å
Zero	-0.204 16) Hartree

Energy Range: 0.90-8.00 Hartree

Table 6: Gives results of curve fitting with modified scattering factors (long-range), EXAFS + XANES range of data (Other parameters fixed at values from Table 4).

"Model Compound": $MnSO_4(NH_4)_2SO_4.6H_2O$ R = 13.4%

Parameters Refined	Values
Limit	2.039 (10) Hartree
Phase adjustment R1	1.143 (19)
Amplitude adjustment R1	2.408 (45)

Energy Range: 0.90-11.95 Hartree.

"Model Compound": $SrBr_2.6H_2O$ R = 22.4%

Parameters Refined	Values
Limit	2.305
Phase adjustment R1	1.92 (2)
Amplitude adjustment R1	8.24 (15)

Energy Range: 0.70-8.20 Hartree

"Model Compound": KBr R = 35%

Parameters Refined	Values
Limit	2.123 (21) Hartree
Phase adjustment R1	2.40 (7)
Amplitude adjustment R1	8.9 (4)
Limit Br-Br	2.81 (11) Hartree
Phase adjustment R2	1.05 (8)
Amplitude adjustment R2	10 (2)

Energy Range: 0.90-8.00 Hartree

Table 7: Gives comparison of the results from $MnSO_4(NH_4)_2SO_4.6H_2O$ and $Mn(NO_3)_2$ solution from "short-range" refinements

Parameters Refined	$MnSO_4(NH_4)_2SO_4.6H_2O$	$Mn(NO_3)_2$ solution
U_1	0.1111 (3) Å	0.103 (1) Å
FP	1.50 (fixed) $Å^{-2}$	1.483 (10) $Å^{-2}$
DelR1	0.326 (1) Å	0.334 (1) Å
R2	4.320 (4) Å	4.397 (4) Å
Zero	0.126 (4) Hartree	0.060 (5) Hartree
MultR2	7 (3)	14 (2)
Residual	7.7%	6.68%

GRAPHS

Figures 12 to 17 represent plots of amplitudes and phases of the elements of our modelled compounds. Figures 18 to 20 represent plots of preliminary least square curve fittings.

Figure 21 is the plot of "long-range" refinement by curve-fitting without scattering factors optimisation while figures 22 to 24 represent plots of radial transform of our EXAFS data in the "long-range" refinement with scattering factors optimisation.

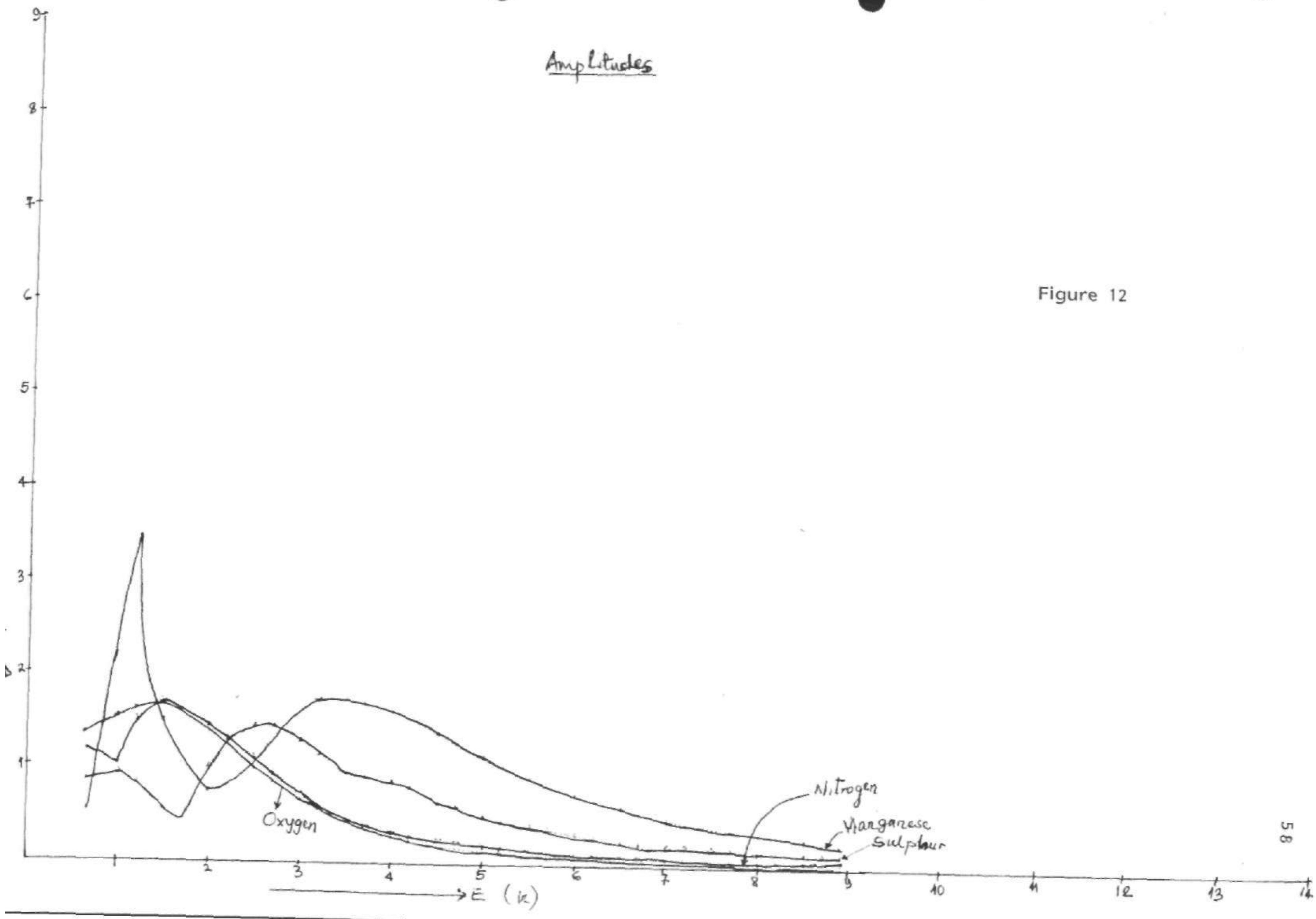
Amplitudes
9
8
7
6
5
4
3
2
1
Oxygen
Nitrogen
Manganese
Sulphur
1
2
3
4
5
6
7
8
9
10
11
12
13
14
E (k)

Figure 12

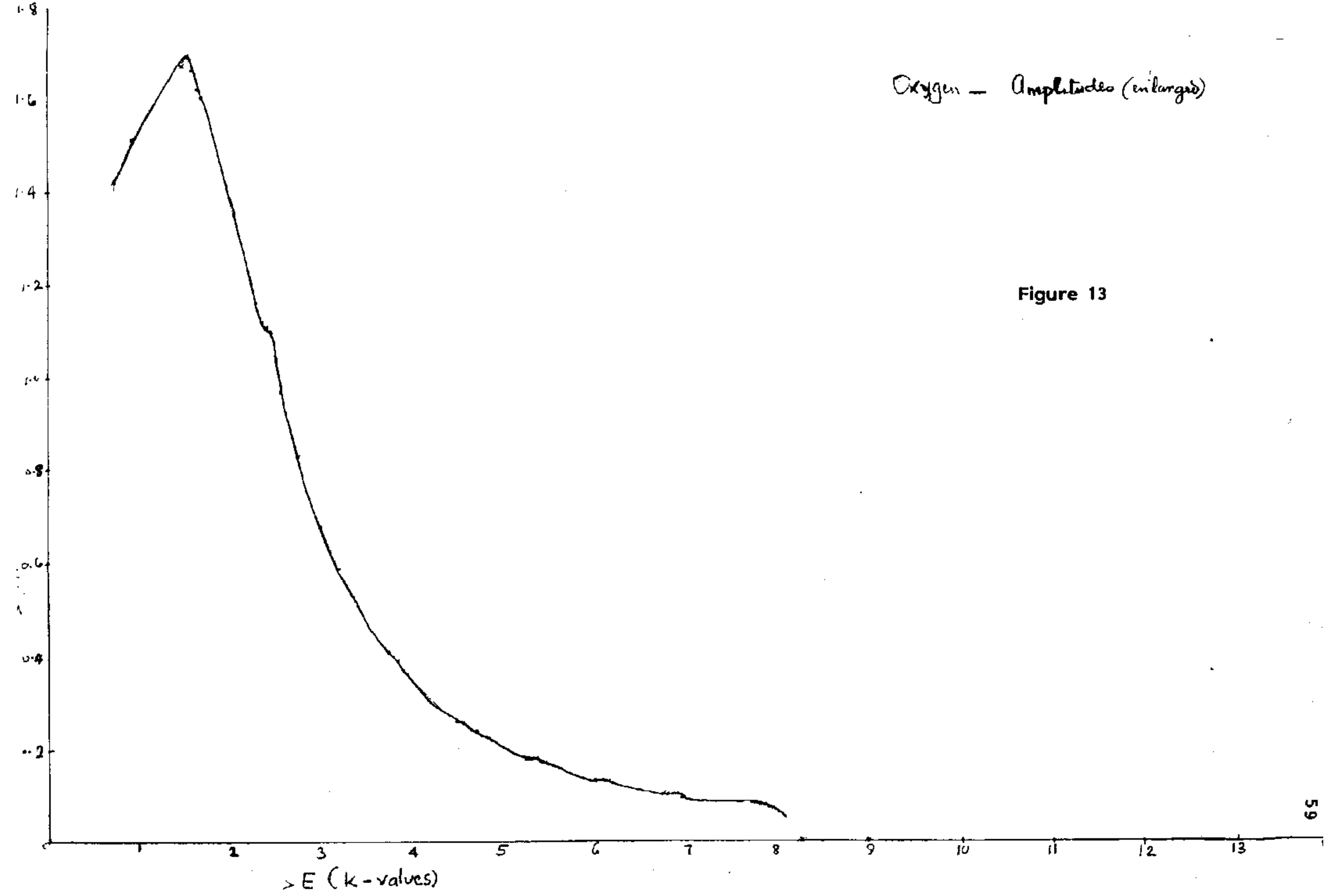
Oxygen — Amplitudes (enlarged)
1·8
1·6
1·4
1·2
1·0
0·8
0·6
0·4
·2
1
2
3
4
5
6
7
8
9
10
11
12
13
> E (k-values)

Figure 13

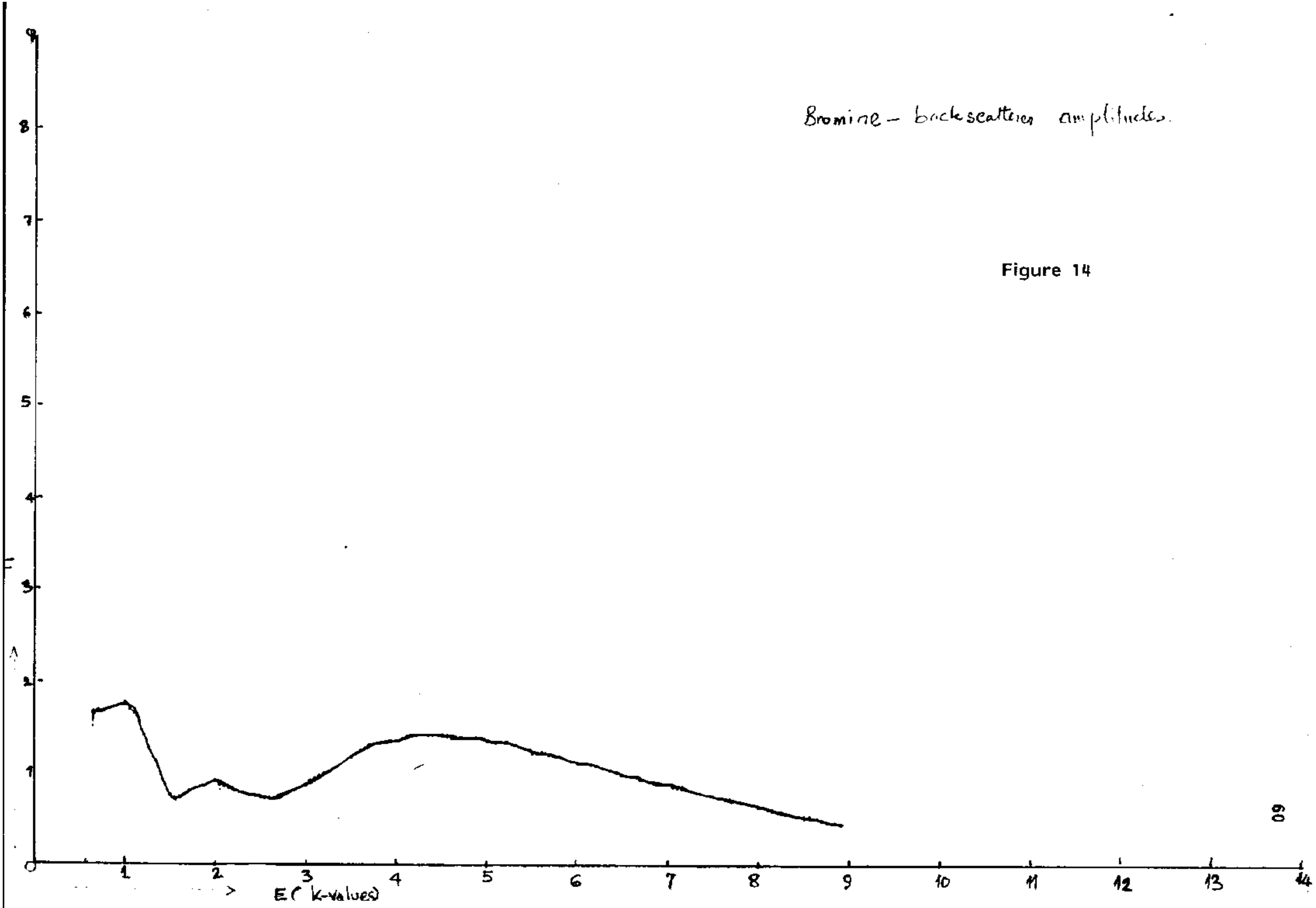
Bromine - backscatterer amplitudes.
E (k-values)
0
1
2
3
4
5
6
7
8
9
10
11
12
13
14

Figure 14

Figure 15

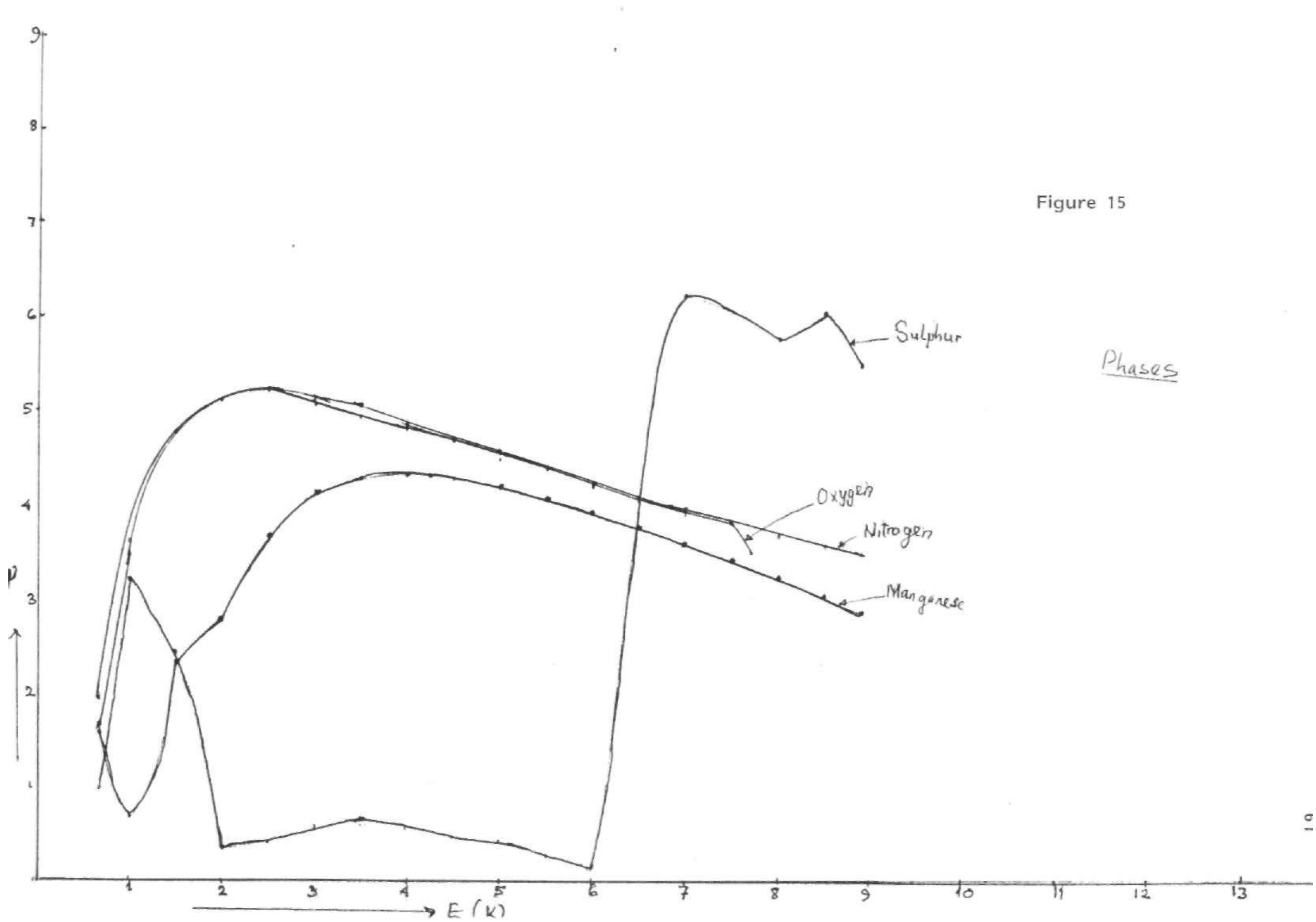

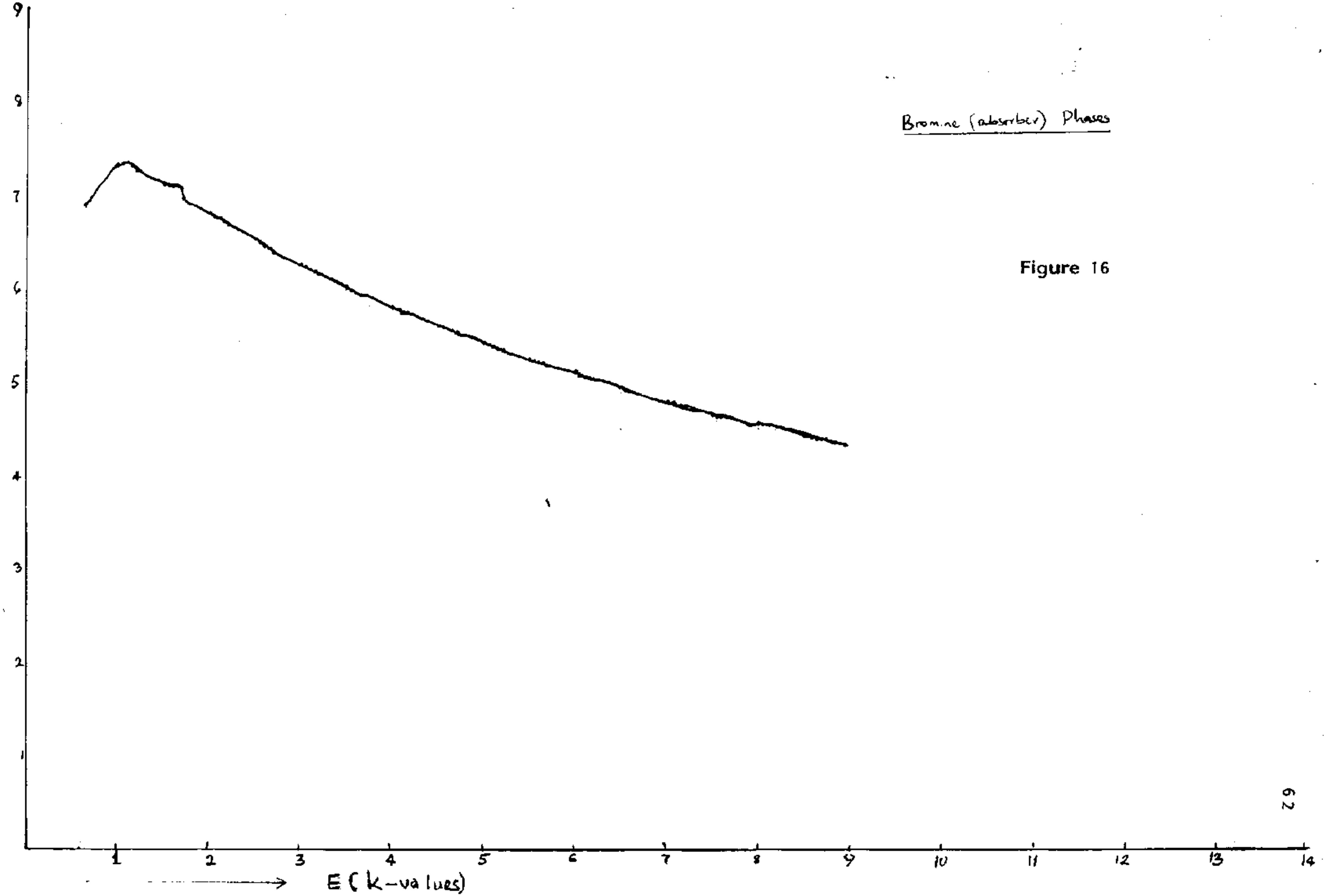
Bromine (absorber) Phases
9
8
7
6
5
4
3
2
1
1 2 3 4 5 6 7 8 9 10 11 12 13 14
E (k-values)

Figure 16

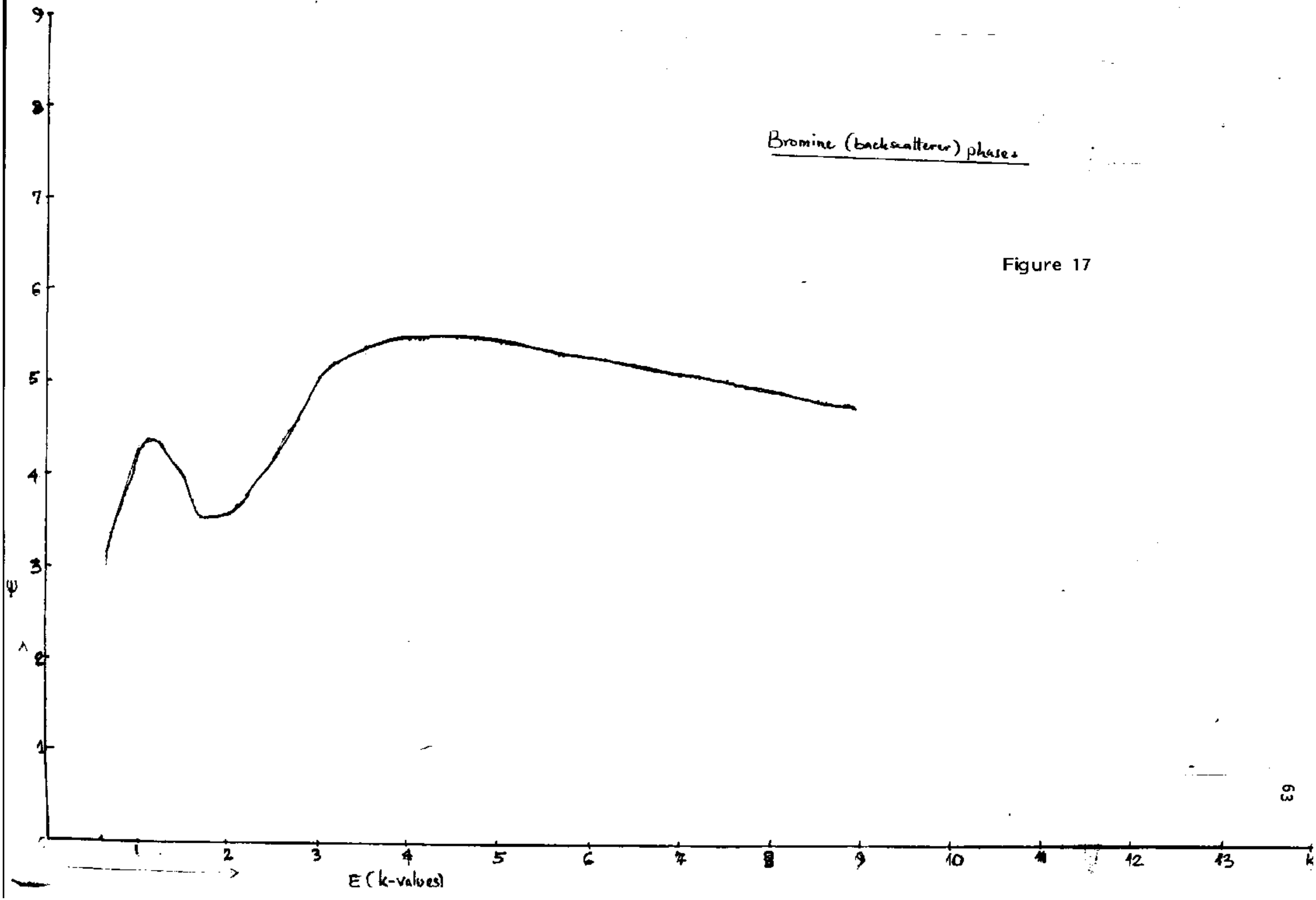
Bromine (backscatterer) phases
ψ
E (k-values)
1 2 3 4 5 6 7 8 9 10 11 12 13 k
1 2 3 4 5 6 7 8 9

Figure 17

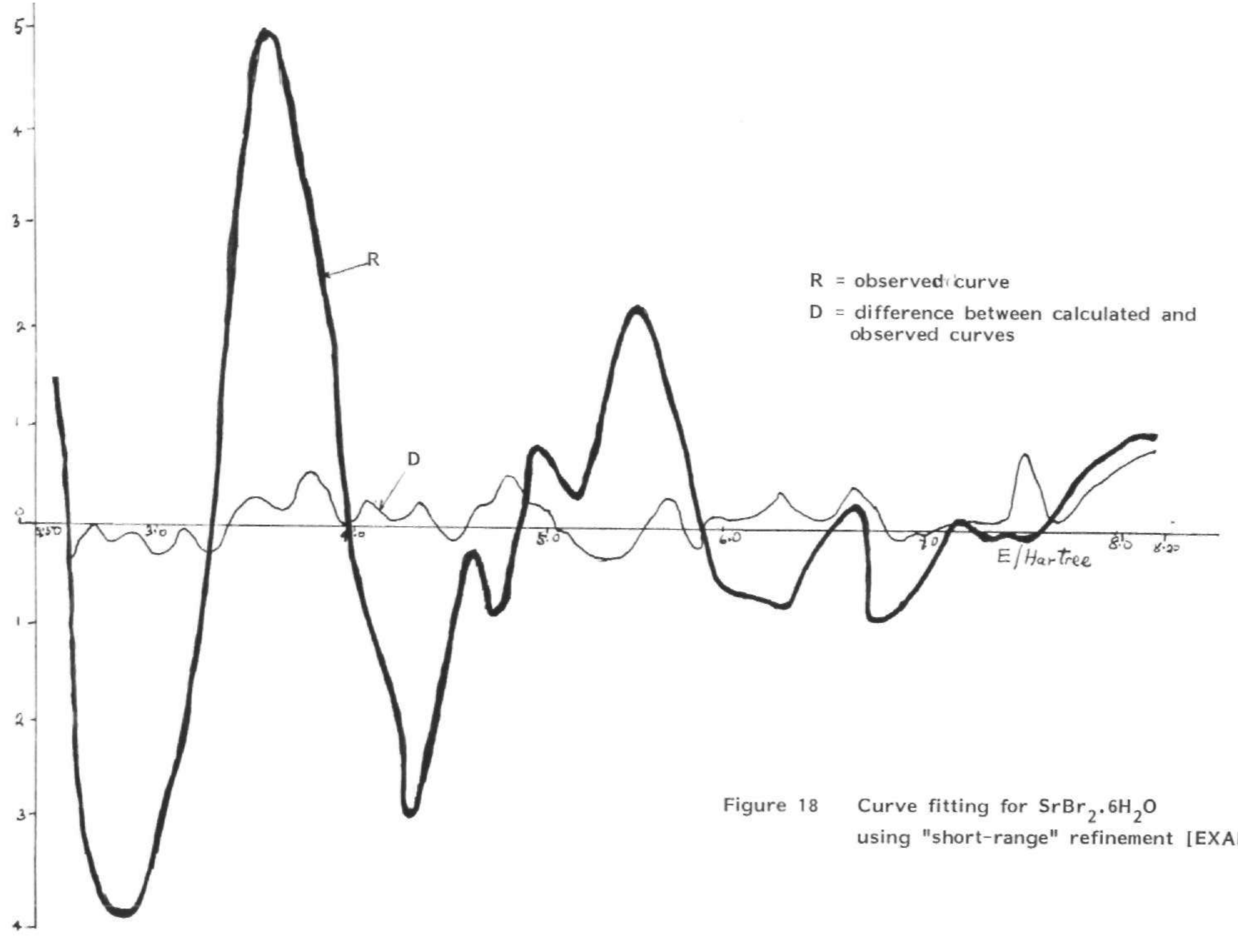

Figure 18 Curve fitting for $SrBr_2.6H_2O$ using "short-range" refinement [EXAFS]

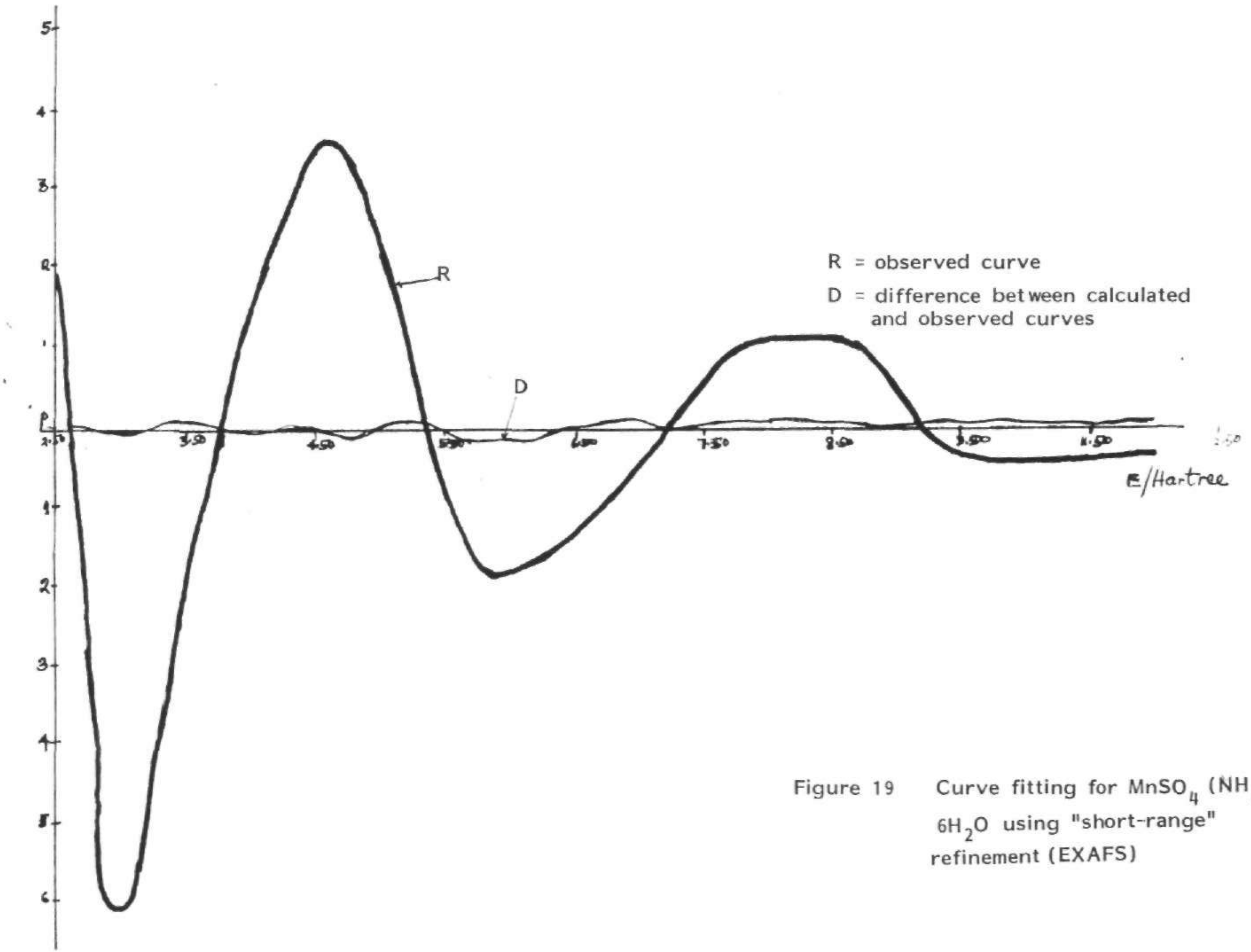

Figure 19 Curve fitting for $MnSO_4\,(NH_4)_2SO_4 \cdot 6H_2O$ using "short-range" refinement (EXAFS)

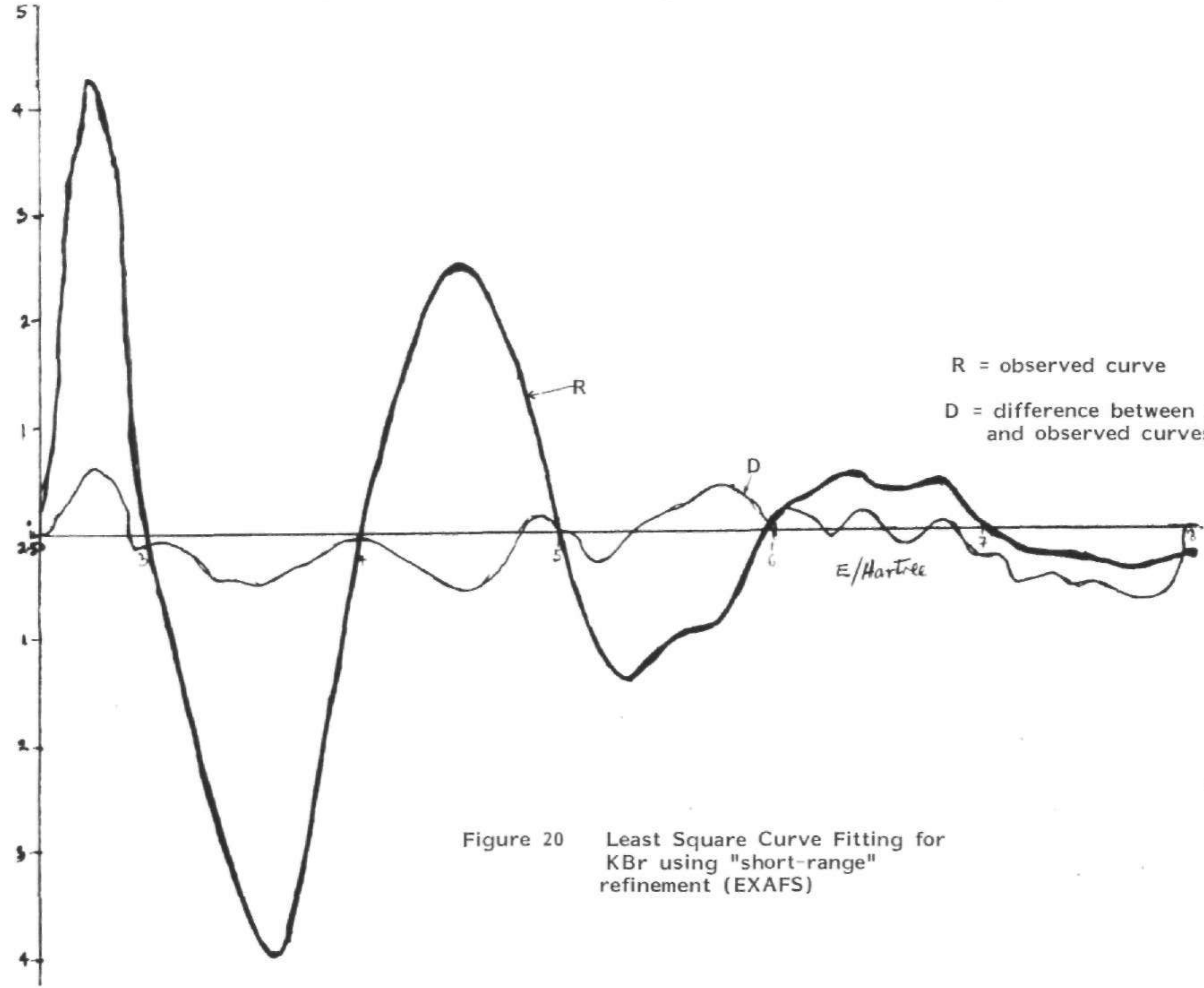

Figure 20 Least Square Curve Fitting for KBr using "short-range" refinement (EXAFS)

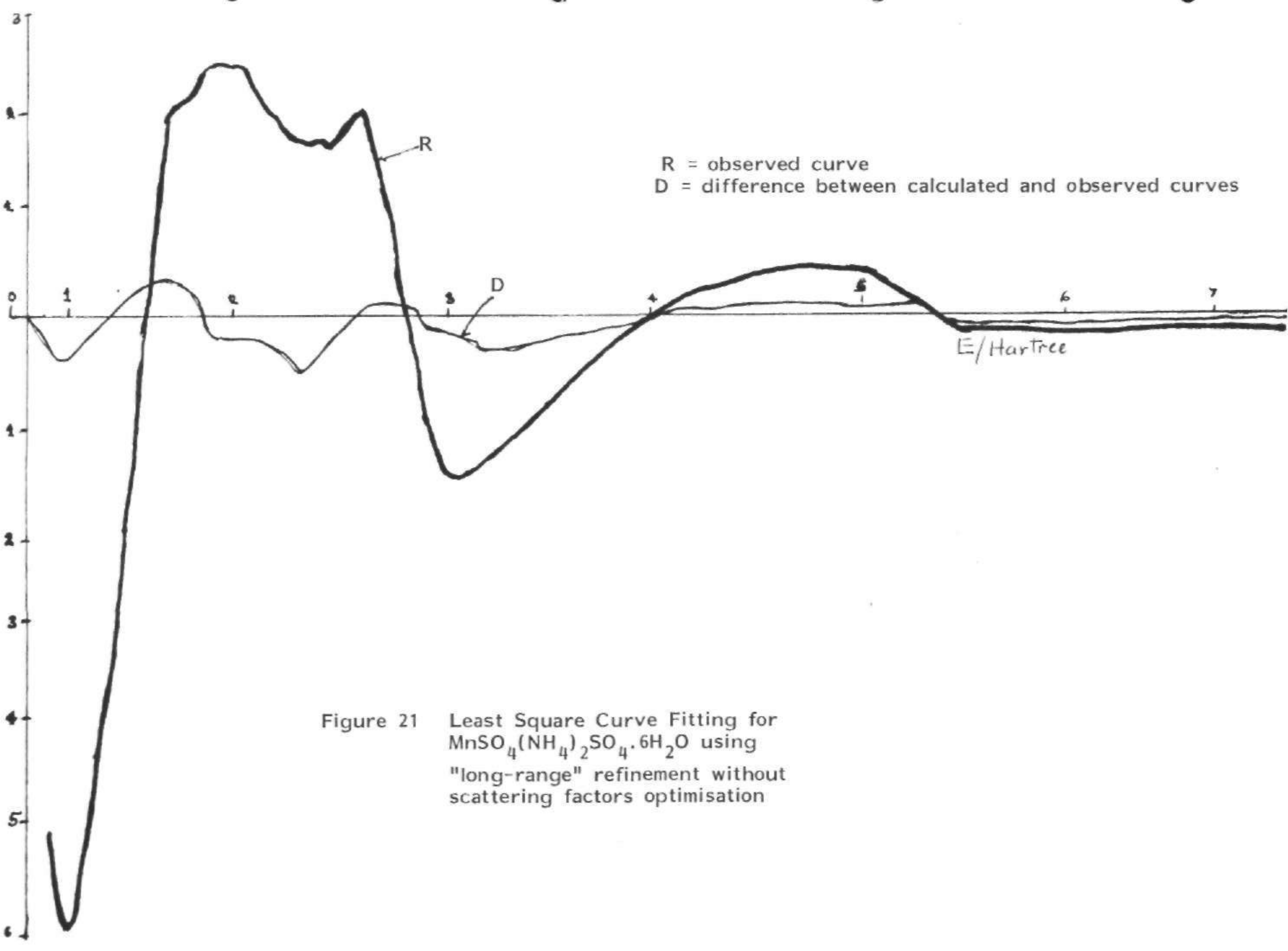

Figure 21 Least Square Curve Fitting for $MnSO_4(NH_4)_2SO_4.6H_2O$ using "long-range" refinement without scattering factors optimisation

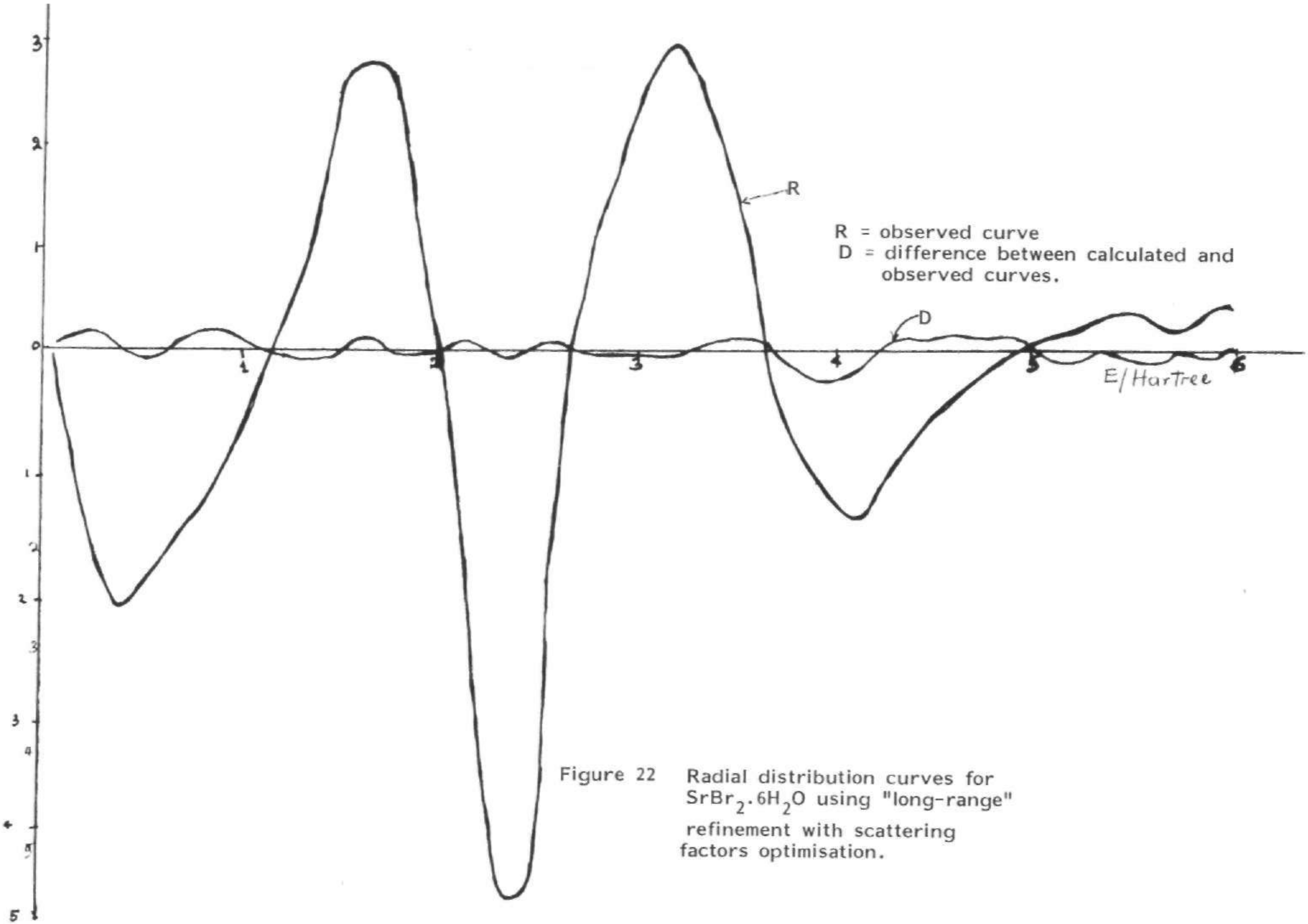

Figure 22 Radial distribution curves for $SrBr_2.6H_2O$ using "long-range" refinement with scattering factors optimisation.

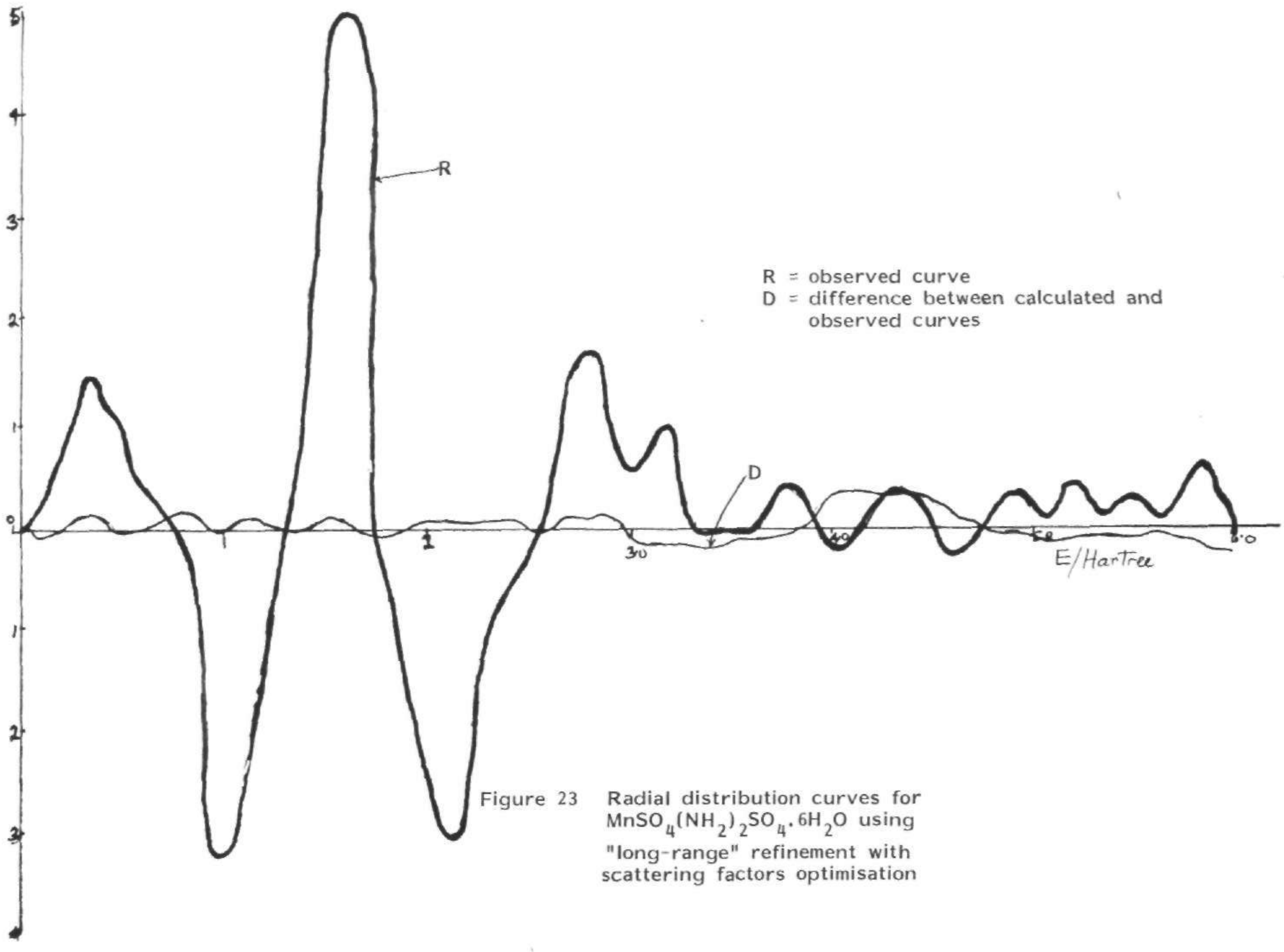

Figure 23 Radial distribution curves for $MnSO_4(NH_2)_2SO_4.6H_2O$ using "long-range" refinement with scattering factors optimisation

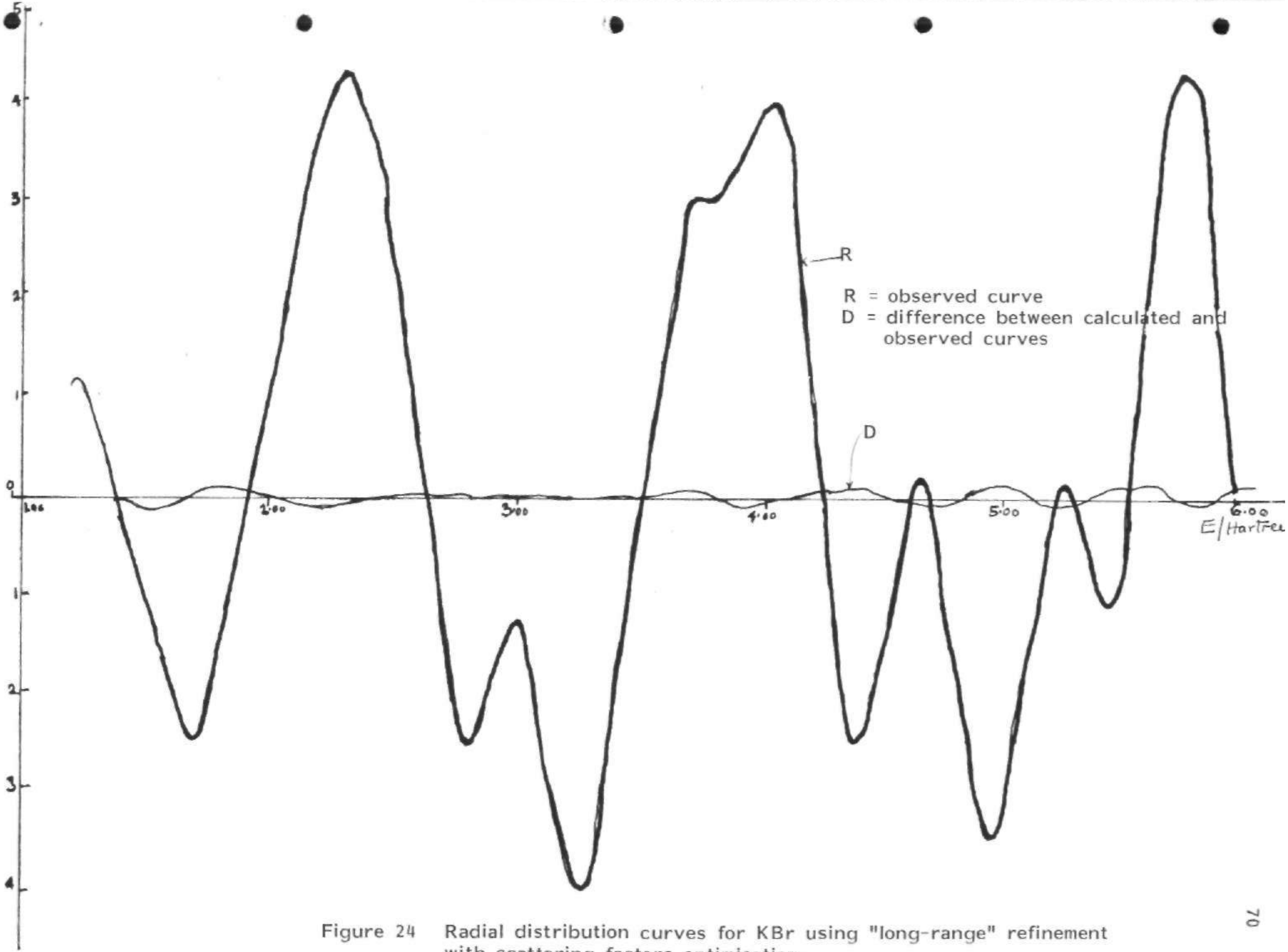

Figure 24 Radial distribution curves for KBr using "long-range" refinement with scattering factors optimisation.

CHAPTER 6

DISCUSSION AND CONCLUSION

CHAPTER 6

DISCUSSION AND CONCLUSION

In many experiments, it is useful to be able to estimate the relative magnitude of the effect of a certain atom would produce on the EXAFS. Scattering factor curves may help such estimations. Figures 12 to 17 represent the plots of the scattering amplitudes and the phases of some of the elements of our compounds. Current theory predicts that the fine structure amplitude due to a particular scattering atom will be proportional to the electron-atom backscattering amplitude $f(\pi,k)$, but diminished by a Debye-Waller like factor $e^{-\sigma^2 ask^2}$. Well beyond the absorption edge $f(\pi,k)$ is smoothly varying and ultimately proportional to Z, the atomic number of the scatterer, while at lower energies (near the edge) $f(\pi,k)$ can show considerable structure. Conversely, differences in σ as have a minor effect at low energies, but completely dominate the spectrum at high k values. Thus, figures 12 to 17 illustrate and quantitatively compare the dramatically different amplitudes for low and high Z elements; plots of $f(\pi,k)$ for Mn, O, S, N were shown in the results. For light atoms such as Oxygen, Sulphur and Nitrogen $f(\pi,k)$ decreases rapidly while heavier elements such as Mn and Br show a pronounced peak in their scattering amplitudes at moderate k values.

At low energies, low Z atoms can actually backscatter more strongly than heavier atoms, and they disproportionately affect the EXAFS in this region.

Theoretically, the total phase shift can be treated as the sum of absorber and scatterer phase shifts. The significant differences in phase shifts in O, S and Mn would permit straightforward differentiation between these atoms as can be seen in Figure 15. On the other hand, it was difficult with the current data to distinguish between atoms with similar phase shifts such as Oxygen and Nitrogen.

Turning to the least-squares curve fitting using the above scattering factors, the refinements carried out in the outer region (EXAFS) gave good fits. This then shows that our assumed scattering factors, obtained with variation of a program called MUFPOT were reasonable for this outer region. The goodness of fit between the theoretical and the experimental data is shown by the low residuals obtained in the process (see Table 4).

An attempt to extend this treatment of the outer region (EXAFS) to the inner (low energy, XANES) region resulted in a bad fit as summarised in Table 5. As can be observed from values presented in this table, there is a poor fit throughout the range of data, residual R = 26% unacceptably different values were obtained for the structural parameters with this method. The major discrepancies occurring in this low energy region are due to uncertainty existing in the behaviour of inelastic and many electron effects. It appeared very unlikely that a good fit can ever be obtained in the inner region with EXAFS unless the scattering factors are properly adjusted.

The third computer treatment incorporated scattering factor adjustment. This version of the program modified the scattering factors in the XANES region and hence maintained a good fit in inner region while keeping the outer region much as before. Table 6 summarises the results from these long-range refinements.

The results in Table 6 compared with those in Table 5 further showed that the existence of a good fit to the data is a necessary (but not sufficient) condition to ensure the correct structural information. The Fourier transformation presented in the results is observed to fit exceedingly well. Successful Fourier transformation is achieved now that a full set of data points has been used.

On the whole, $MnSO_4(NH_4)_2SO_4.6H_2O$ has been observed to show better residuals of fit both in the "long-range" and in the "short-range" refinements. This is followed by $SrBr_2.6H_2O$ and lastly the KBr. This difference in residuals is due to the greater noise in the Br- edge data - present for experimental reasons.

Table 7 demonstrates the applicability of EXAFS technique to structure determinisation. The agreement between structural results obtained from $MnSO_4(NH_4)_2SO_4.6H_2O$ and $Mn(NO_3)_2$ solution having similar absorber atoms is most intriguing, and at the same time shows the level of transferability possible.

The long-range refinements have actually optimised the scattering factors in the XANES region and we hope the present method will extend the applicability of EXAFS in structure determinations of unknown compounds. Furthermore, the investigation has succeeded in producing values for the vibrational amplitudes U_1 (and U_2) and DELR values and the scattering factor modification parameters; all these can be carried over and regarded as fixed in determining the structure of an unknown compound.

The fact that we have succeeded in obtaining good fit with both the "short-range" and the "long-range" (with corrected scattering factors) refinements show that the methods used in this investigation proved successful (i.e. that the objectives outlined at the outset of the work have been largely achieved).

Finally, continuing improvements in both the analysis and the computing procedures ("short- and long-range" refinements) and in the experimental sensitivity should make EXAFS an important tool in many structural investigations.

The date presented here show that the Extended X-ray Absorption Fine Structure (EXAFS) can be used with appropriate calibration parameters to characterise distances of scattering atoms and other structural parameters. It is particularly capable of closing this for the absorber's first coordination sphere. In this regard, the future of EXAFS spectroscopy is as bright as the future of the synchrotron radiation source.

The EXAFS of $MnSO_r(NH_4)_2SO_4.6H_2O$, KBr and $SrBr_2.6H_2O$ have been analysed by a method which combined Fourier transform and

Curve-fitting techniques. Essentially, we have employed for convenience, "short-range" and "long-range" in our computing procedures. This has been shown to work well. This work supports the conclusion of Pettifer et al[109] in analysing different factors making the scattering factors in the XANES difficult to understand.

The results obtained demonstrate the applicability of EXAFS to structural determination, and its potential for the study of unknown structures with similar elements to those used in the present investigation.

REFERENCES

1. Roetgen, W.C., Ann. Phys. 64 (1895) 1
2. Friedrich, W., Knipping, P. et al, Akad. Wiss. (1912), pp. 303-12.
3. Bragg, W.L., Proc. Cambridge Philos. Soc. 17 (1912): 43.
4. De Broglie, M., Comptes Rendus 157 (1913): 924-26.
5. Frickie, H., Phys. Rev. 16 (1920): 202-15.
6. Hertz, G., Phys. Z. 21 (1920): 630-32
7. Lindh, A.E., Z. Phys. 6 (1925): 303-10.
8. Lindsay, G.A. Comptes Rendus, 175 (1931):150-51.
9. Coster, D., Z. Phys. 25 (1931): 83-98.
10. Kronig, R. de L. Z. Phys. 70 (1932): 317-23.
11. Bloch, F. Z. Phys. 52 (1928): 555-600.
12. Davisson, C.J., Germer, L.H., Phys. Rev. 30 (1928): 705-40.
13. Rupp, E. Ann. Phys. 5 (1930): 453-74.
14. Hayasi, T., Sci. Rep. Tohoku, Univ. Ser. 1, 33 (1949): 183-94.
15. Hanawalt, J.D., Phys. Rev. 37 (1931): 715-26.
16. Kronig, R. de L. Z. Phys. 75 (1932): 468-75.
17. Peterson, H. Z. Phys. 76 (1932): 768-76.
18. Kostarev, A.I., Zh. Eskp. Teor. Fiz. 11 (1941): 60.
19. Peterson, H., Ibid, 76 (1932): 768-76.
20. Kozlenkov, A.I., Izv. Akad. Nauk. SSSR 25 (1961): 957.
21. Sawada, M., J. Phys. Soc. Jpn., 12 (1957): 788-92.
22. Hanawalt, J.D., Z.Phys. 70 (1931): 293-305.
23. Lytle, F.W., Advances in X-ray Analysis, ed. (1966): pp.544.
24. Lytle, F.W.,

25. Prins, J.A., Physics of Non-crystalline solids, (1965), pp. 12-30.

26. Sayers, D.E., Lytle, F.W., Stern, E., Advances in X-ray Analysis (1970): pp. 681.

27. Sayers, D.E., Stern, E.A., Lytle, F.W., Phys. Rev.,Lett. 27 (1971): 1204-7.

28. C. Kunz, Topics in Current Physics, Synchrotron Radiation (1979), pp. 3.

29. Eisenberger, P., Brown, G.S., Solid State Commun. 29(6) (1974):481-4.

30. Boon-Keng Teo, EXAFS Spectroscopy: Techniques and Applications, pp. 44.

31. Boon-Keng Teo, Ref. 30, pp. 46.

32. Boon-Keng Teo, Ref. 30, pp. 47.

33. Boon-Keng Teo, Ref. 30, pp. 48.

34. Boon-Keng Teo, Ref. 30, pp. 49.

35. Boon-Keng Teo, Ref. 30, pp. 50.

36. Lectures taken during a discussion session held at Daresbury, Warrington.

37. Beagley, B., Gahan, B., et al, UMIST, Unpublished Results.

38. Huckins, G.N., M.Sc. Thesis, 1982.

39. Rabe, P. et al, Solid State Phys., 12 1173 (1979).

40. El. Saffar G.M. Brown, Acta. Cryst. B27 (1971), 66.

41. Brian Beagley, Brendan Gahan et al., J. Chem. Soc., Chem. Commun. (1983), 1265.

42. Stohr, J. et al, Phys. Rev. B20 (1979): 664.

43. Beagley, B., Ganan, B. et al, Ref. 37.

44. Apte, M.Y., Mande, C., J. Phys. Chem. Solids 41 (1980): 307.

45. Rabe, R., Tolkiehn, G., Werner, A., J. Phys. Chem. 12(6) (1979), 1173-81.

46. Rabe, P., Tolkiehn, G. et al, Phys. Chem. 12 (1974): 899, ibid, 12 (1979): 11.73.

47. Apte, M.Y., et al, Ref. 44, pp. 308.

48 Crozier, E.D., Alberding, N.A. et al, J. Chem. Phys. 79(2) (1983): 939-43.

49. Sandstrom, D.R., J. Chem. Phys., 71, (1979): 2381.

50. Stern, E.A., Heald Steve M., Rev. Sci. Instru., 50 (1979): 1571.

51. Verdaguer, M. et al, Inorganic Chem. 19 (1980): 3271.

52. Stern, E.. et al, Phys. Rev. Lett. 42 (1979): 1372.

53. Sukhorukov, V.L., Demekhina, L.A., et al, Soviet Phys. Solid State, 21 (1979): 2976.

54. El. Saffar et al, Ref. 40, pp. 67.

55. Galli, G.,et al, Solid State Comm., 42(3) (1982): 213.

56. Stern, E.A., Bruker, B.A., et al, Phys. Rev., B21 (1980): 552.

57. Hayes, T.M., J. Non-Cryst. Solids 31 (1-2) (1978): 57-79.

58. Sukhorukov, L.A. et al, Fiz. Tverd, Tala(Leningrad) 21 (1979): 2976.

59. Chastain, R.V. et al, Acta. Cryst. 20 (1966): 731.

60. Ibid, 20 (1966): 732.

61. Zalkin,Forrester and Templeton, Inorg. Chem. 3 (1964): 529.

62. Hermann, Z. Anorg. Allgem. Chem. 196, 79.

63. Jensen, A.T., Danske Vid. Selsk. Mat. Fys. Medd. 17, No. 9 (1940).

64. Ibid, 17, No. 9 (1940), pp. 8.

65. Bernal, J.D., Fowler, R.H., J. Chem. Phys. 1 (1933): 515.

66. Le Claire and Borel, Acta. Cryst. B33 (1977): 2938-40.

67. Ruth, W., Z. Phys. 143, (1956): 591-604.

(ii) Akinsin, P.A. et al, Z. Neorg. Khim. 4 (1959), 718-723.

(iii) Report Project, National Bureau of Standards, U.S. Circular 539, 1 (1956): 66.

68. Ruth, W., Ref. 67(i), pp. 719.

69. De Cugnac., Pouradier, J. Acad. Sci. Paris, 258, 4768.

70. R. de L. Kronig, Z. Phys., 70 (1931): 317.

71. Lee, P.A., Ref. 30, pp. 5.

72. Sayers, D.E., Stern, E.A. et al, Phys Rev. Lett. 27 (1971): 1207.

73. Lee, P.A., Ref. 30, pp. 6.

74. Lee, P.A. idem, pp. 6.

75. Lee, P.A. idem, pp. 7.

76. Lee, P.A. and Citrin, P.H. et al, Unpublished.

77. Teo, B.K., and Lee, P.A., J. Am. Chem. Soc., 101 (1979): 2815.

78. Lee, P.A., Beni, G., Phys. Rev. B15 (1977): 2862.

79. Lee, P.A. et al, Ref. 20, pp. 6.

80. Lee, P.A. et al, Ref. 30, pp. 7.

81. Lee, P.A. et al, Ref. 30, pp. 7.

82. Lee, P.A. and Pendry, J.B., Phys. Rev., B11, (1975): 2795.

83. Teo, B.K., andJoy, D.C. EXAFS Spectroscopy (Plenum), pp. 6.

84. Lee, P.A., and Beni, G., Phys. Rev., B15 (1977): 2862.

85. Stern, E.A., Sayers, D.E. et al, Phys. Rev. B11 (1975): 4836.

86. Lytle, F.W., Sayers, D.E. et al, Phys. Rev. B11 (1975): 4825.

87. Citrin, P.H., Eisenberger, P., Phys. Rev. Lett. 36 (1976): 1346.

88. Lee, P.A. and Beni, G., Phys. Rev. B15 (1977): 2862.

89. Rehr, J.J., Stern, P.L. et al, Phys. Rev. B17 (1978): 560.

90. Stern, E.A., and Heald, S.M., Rev. Sci. Instr. 50 (1979): 1579.

91. Stern, E.A., Bunker, B. et al, Phys. Rev., B21 (1980): 5521.

92. Eisenberger, P., and Brown, G., Sold State Comm. 29 (1979): 481.

93. Hayes, T.M., Boyce, J.B., J. Phys. C11 (1978): 2931.

94. Eisenberger, et al, Ref. 92.

95. Eisenberger, et al, Ref. 92

96. Schmidt, V.V., Bull. Acad. Sci. USSR, Ser. Phys. 25 (1961): 998.

97. Idem, 27 (1963): 392.

98. Beni, G. and Platzman, P.M., Phys. Rev. B14 (1976): 1514.

99. Sevillano, E.H., Meuth et al, Phys. Rev. B20 (1979): 4908.

100. Rehr, J.J., Stern, E.A., Phys. Rev. B17 (1978): 560.

101. Idem 74 (1974): 1853.

102. Rabe, P., Tolkiehn, G. et al, J. Phys, C12 (1979): L545.

103. Böhmer, W., and Rabe, P. J. Phys. C12 (1979): 2465.

104. Eisenberger, P., Shulman, R.G., Nat. Acad. Sci., U.S.A. 73 (1976): 491.

105. EXAFS for Inorganic Systems, Proceedings of the Daresbury Study Weekend, March 1981.

106. Martens, G. et al., J. Phys. C11 (1977): 3125.

107. McMaster, N., Kerr del Grande, et al., Computations of X-ray Cross Sections (1969), UCRL-50174.

108. Cramer, S.P., Eccles, T.K., et al., J. Am. Soc. 98 (1976): 8059.

109. Bianconi et al., EXAFS and Nuclear Edge Structure, Plenum (1983): p. 66.

BIBLIOGRAPHY

1. EXAFS Spectrscopy Techniques and Applications by B.K. Teo and D.C. Joy (Plenum), December, 1980.
2. EXAFS and Nuclear Edge Structure, Chemical Physics, Series 27 by Bianconi, L. Incoccia and S. Stipcich, New York, Tokyo (1983).
3. Synchrotron Radiation Research by Winicle Doniach, Plenum Press (1980).
4. Handbook on Synchrotron Radiation by E. E. Koch, Volumes I and II, Plenum Press (1983).

COMPUTER PROGRAMME USED IN THE EARLY PART OF THE INVESTIGATION.

```
15/10/84  13:47:55                    ___R0000E A*S___                 PAGE  1

//E3500 JOB ,'MCD3500',CLASS=Y
**JOB B3500,MCD3500,ST=(MFZ,SF,MS150000),C=0,TI=150,PW=MCD3500,
/* OUTPUT=(SYSOUT=A,DEST=MCU,HOLD=YES)
LIBRARY,PROCLIB.
NEWPROC.
GETFEP,XAF,S:MC.0000.ESTRICOTI,FD=BINARY.
GETFEP,A,KBRRAND.
REWIND,XAF,A.
FTN.
LISEDT.
RETURN,LGO.
REWIND,DEPEND.
LIBRARY,DEPEND.
XAF,PL=100000.
REWIND,RAND,INPUT.
COPYSP,INPUT,OUTPUT.
EXIT,U.
####S
      SUBROUTINE DEPEND(IWR)
      COMMON/WORK/DUMP(4540),R(200),U(200),NEXT(1500),V(100),IV(100),
     1X(100),Y(100),Z(100),NO(100),REST(3890),MOLFRA(4,10),SC(4),
     2Q(152),ZERO,ETA,CN(200),NSF,NDATA,USER(490)
      REAL MOLFRA
      IF(IWR.EQ.1) WRITE(2,100)
 100  FORMAT(1H0,4X,'USER FOR KBR ')
      N=5
      LV=1
      DO 99 L=1,N
      R(L)=V(LV)
      U(L)=V(LV+1)
      USER(10+L)=V(LV+2)
      USER(20+L)=V(LV+3)
      USER(30+L)=V(LV+4)
      USER(40+L)=V(LV+5)
   99 LV=LV+6
      ZERO=V(LV)
      RETURN
      END
      FUNCTION USERSF(FJ,EJ,SH,SK,IJ)
      COMMON/WORK/RA(200),DUMA(4540),U(200),DUMB(5470),USER(490)
      F=-FJ*USER(10+IJ)*SIN(2.0*SK*RA(IJ)+SH+EJ+USER(20+IJ)-0.32*SK)
      FP=2.0*RA(IJ)*USER(30+IJ)/(SK**USER(40+IJ))
      F=F*EXP(-0.5*U(IJ)*U(IJ)*SK*SK-FP)
      USERSF=F/(SK*RA(IJ)**2)
      RETURN
      END
####S
LIBRARY(DEPEND,NEW)
REWIND(LGO)
ADD(*,LGO)
FINISH.
####S
??INRAND(IN1=A,IN2=4)
??INRAND(IN1=A,IN2=4)
??INRAND(IN1=A,IN2=4)
??INRAND(IN1=A,IN2=4)
??INRAND(IN1=A,IN2=4)
??INRAND(IN1=A,IN2=4)
```

```
??INRAND(IN1=A,IN2=A)
??INRAND(IN1=A,IN2=A)
??INRAND(IN2=CR)
  22    2   2                                                       1    0(0=10.5)
   0.24517    0.03000   15.00017
??EXAFSLS2(OUTJ=LP)
    KBR
V/  1    2.702   0 R1?
V/  2    0.112   0 U1
V/  3    6.000   0 MULT R1
V/  4    0.000   0 PHASE R1
V/  5    1.500   0 FP R1?
V/  6    1.000   0 F-P POWER R1
V/  7    2.691   0 R2
V/  8    0.149   0 U2
V/  9    0.000   0 MULT R2?
V/ 10    0.000   0 PHASE R2
V/ 11    1.500   0 F-P R2
V/ 12    1.000   0 F-P POWER R2
V/ 13    3.650   0 R3?
V/ 14    0.167   0 U3
V/ 15    0.000   0 MULT R3
V/ 16    0.000   0 PHASE R3
V/ 17    1.500   0 FP R3?
V/ 18    1.000   0 FP POWER R3
V/ 19    0.006   0 ZERO
R/  1   1   1   1  19
R/  2   1   1   1  19
R/  3   1   1   1  19
SPDELK=  1 X 19,  1 X 35,  1 X  1
DATA/E= 1
TSAVER= 1
SHIFTX=0.01
CYCLES= 1
SCALES= 1.00    1
RADIAL DISTRIBUTION/M=  3,N=  3,DELR=0.050,RMAX= 6.00,CONST=0.010
LS END
??EXAFSCONT(LPPLOT,OUT3=LP)
UPHSCL=1.0
BCKGND/          2.50    5.00        0/USE CURVE 1 IN RAND
FTCORR=          1.0     1.0
??EXAFSLS2(OUT3=LP)
SHIFTX=0.2
TSAVER= 0
CYCLES=20
SCALES= 1.00    0
V/  1    2.702   1 R1
V/  2    0.112   1 U1=U2
V/ 19    0.006   0 ZERO
??EXAFSCONT(LPPLOT,OUT3=LP)
FTCORR=3.0      1.0     1.0
BCKGND/          2.50    5.00        1/USE CURVE 1 IN RAND
??EXAFSLS.(OUT3=LP)
TSAVER= 0
SCALES= 1.00    0
V/ 19    0.006   1 ZERO
??EXAFSCONT(LPPLOT,OUT3=LP)
```



```
FTCORR=3.0      1.0     1.0
??END.
```

THE SECOND VERSION OF THE COMPUTER PROGRAMME.

```
16/10/84   15:51:53                      ___ROSCOE AWS___                        PAGE

//B3BBR JOB ,'MODSDDD',CLASS=Y
**JOB B3BBR,MODSSDD,ST=(MFI,SP,4516DDDD),D=D,TI=150,PW=MODSDDD,
/* OUTPUT=(SYSOUT=A,DEST=MDD,HOLD=YES)
LIBRARY,PROCLIB.
NEWPROC.
GETFEP,XAF,$:MC.DSSBG.BBTRICOTS,FD=BINARY.
GETFEP,A,$:MC.DSSSG.BBRAND2(RAND)$.
REWIND,XAF,A.
FTN.
LIBEDT.
RETURN,LGO.
REWIND,DEPEND.
LIBRARY,DEPEND.
XAF,PL=100000.
REWIND,RAND,INPUT.
COPYSP,INPUT,OUTPUT.
EXIT,U.
####S
      SUBROUTINE DEPEND(IWR)
      COMMON/WORK/DUMP(4640),R(200),U(200),NEXT(1600),V(100),IV(100),
     1X(100),Y(100),Z(100),NO(100),REST(3890),MOLFRA(4,10),SC(4),
     2Q(132),ZERO,ETA,CN(200),NSF,NDATA,USER(490)
      REAL MOLFRA
      IF(IWR.EQ.1) WRITE(2,100)
 100  FORMAT(1H0,4X,'SUBR FOR KBR ')
      V(15)=V(25)=V(35)=V(5)
      V(12)=V(2)
      V(32)=V(22)
      V(27)=V(7)
      V(37)=V(17)
      N=4
      LV=1
      DO 99 L=1,N
      R(L)=V(LV)
      U(L)=V(LV+1)
      USER(10+L)=V(LV+2)
      USER(20+L)=V(LV+3)
      USER(30+L)=V(LV+4)
      USER(40+L)=V(LV+5)
      USER(50+L)=V(LV+6)
      USER(60+L)=V(LV+7)
      USER(70+L)=V(LV+8)
      USER(80+L)=V(LV+9)
   99 LV=LV+10
      ZERO=V(LV)
      RETURN
      END
      FUNCTION USERSF(FJ,EJ,SH,SK,IJ)
      COMMON/WORK/RA(200),DUMA(4640),U(200),DLMB(5470),USER(490)
      ANG=2.0*SK*(RA(IJ)-USER(50+IJ))+SH+EJ+USER(20+IJ)
      F=-FJ*USER(10+IJ)*SIN(ANG)
      FP=2.0*RA(IJ)*USER(30+IJ)/(SK**USER(40+IJ))
      F=F*EXP(-2.0*U(IJ)*U(IJ)*SK*SK-FP)
      USERSF=F/(SK*RA(IJ)**2)
      RETURN
      END
####S
LIBRARY(DEPEND,NEW)
```

```
END
####S
LIBRARY(DEPEND,NEW)
```



```
REWIND(LGO)
ADD(*,LGO)
FINISH.
####S
??INRAND(IN1=A,IN2=A)
??INRAND(IN1=A,IN2=A)
??INRAND(IN1=A,IN2=A)
??INRAND(IN1=A,IN2=A)
??INRAND(IN1=A,IN2=A)
??INRAND(IN1=A,IN2=A)
??INRAND(IN1=A,IN2=A)
??INRAND(IN1=A,IN2=A)
??INRAND(IN1=A,IN2=A)
??INRAND(IN2=CR)
  02   2   2                              R              1   3(3F10.5)
   0.24317   0.00000   15.55317
??EXAFSLS.(OUTS=LP)
     KBR
V/  1    3.299   0 R1?
V/  2    0.147   0 U1
V/  3    0.000   0 MULT R1
V/  4    0.000   0 PHASE R1
V/  5    1.500   0 FP R1?
V/  6    1.000   0 F-P POWER R1
V/  7    0.450   0 DELR1
V/  8    0.000   0 UNUSED
V/  9    0.000   0 UNUSED
V/ 10    0.000   0 UNUSED
V/ 11    2.591   0 R2
V/ 12    0.149   0 U2
V/ 13    0.000   0 MULT R2?
V/ 14    0.000   0 PHASE R2
V/ 15    1.500   0 F-P R2
V/ 16    1.000   0 F-P POWER R2
V/ 17    0.400   0 DELR2
V/ 18    0.000   0 UNUSED
V/ 19    0.000   0 UNUSED
V/ 20    0.000   0 UNUSED
V/ 21    3.550   0 R3?
V/ 22    0.167   0 U3
V/ 23    0.000   0 MULT R3
V/ 24    0.000   0 PHASE R3
V/ 25    1.500   0 FP R3?
V/ 26    1.000   0 FP POWER R3
V/ 27    0.400   0 DELR3
V/ 28    0.000   0 UNUSED
V/ 29    0.000   0 UNUSED
V/ 30    0.000   0 UNUSED
V/ 31    4.000   0 R4
V/ 32    0.100   0 U4
V/ 33    0.000   0 MULT R4
V/ 34    0.000   0 PHASE R4
V/ 35    1.500   0 FP R4
V/ 36    1.000   0 FP POWER R4
V/ 37    0.400   0 DELR4
V/ 38    0.000   0 UNUSED
V/ 39    0.000   0 UNUSED
V/ 40    0.000   0 UNUSED
```

```
V/ 41   0.142  0 ZERO
R/  1   1   1   1 19
R/  2   1   1   1 19
R/  3   1   1   1 19
R/  4   1   1   1 19
SFDELK=  1 X 19,  1 X 35,  1 X  1
DATA/E= 1
TSAVER= 1
SHIFTX=0.01
CYCLES= 1
SCALES= 1.00    1
RADIAL DISTRIBUTION/M=  3,N=  5,DELR=0.050,RMAX= 6.00,CONST=0.010
LS END
??EXAFSCONT(LPPLOT,OUT3=LP)
UPHSCL=1.0
BCKGND/        2.50    3.00      0/USE CURVE 1 IN RAND
FTCORR=        1.0     1.0
??EXAFSLSQ(OUT3=LP)
SHIFTX=0.2
TSAVER= 0
CYCLES=20
SCALES= 1.00    0
V/  7   0.430  1 DELR1
V/  2   0.147  1 U1=U2
V/ 41   0.142  0 ZERO
??EXAFSCONT(LPPLOT,OUT3=LP)
FTCORR=3.0     1.0     1.0
BCKGND/        2.50    3.00      1/USE CURVE 1 IN RAND
??EXAFSLSQ(OUT3=LP)
TSAVER= 0
SCALES= 1.00    0
V/ 41   0.142  1 ZERO
??EXAFSCONT(LPPLOT,OUT3=LP)
FTCORR=3.0     1.0     1.0
??END.
####S
```

THE FINAL VERSION OF THE COMPUTER PROGRAMME.

```
16/10/84  15:53:16                    ___ROSCOE AWS___                    PAGE

//BBBMNNEW JOB ,'MCDSSBO',CLASS=Y
**JOB BBBMNNEW,MCDSSBO,ST=(MFZ,SP,MS150000),C=C,TI=150,PW=MCDSSBO,
/* OUTPUT=(SYSOUT=A,DEST=MCD,HOLD=YES)
LIBRARY,PROCLIB.
NEWPROC.
GETFEP,XAF,$:MC.DSSBG.BBTRICOTE,FD=BINARY.
GETFEP,A,$:MC.DSSBG.BBRANDD(R5332)B.
REWIND,XAF,A.
FTN.
LIBEDT.
RETURN,LGO.
REWIND,DEPEND.
LIBRARY,DEPEND.
XAF,PL=100000.
REWIND,RAND,INPUT.
COPYSP,INPUT,OUTPUT.
EXIT,U.
####S
      SUBROUTINE DEPEND(IWR)
      COMMON/WORK/DUMP(4640),R(200),U(200),NEXT(1600),V(100),IV(100),
     1X(100),Y(100),Z(100),NO(100),REST(3390),MOLFRA(4,10),SC(4),
     2Q(132),ZERO,ETA,CN(200),NSF,NDATA,USER(490)
      REAL MOLFRA
      IF(IWR.EQ.1) WRITE(2,100)
  100 FORMAT(1H0,4X,'SUBR FOR MNSO4.(NH4)2SO4.6H2O ')
      V(15)=V(25)=V(35)=V(5)
      V(40)=V(30)=V(20)=V(10)
      V(39)=V(29)=V(19)=V(9)
      V(36)=V(26)=V(16)=V(6)
      V(12)=V(2)
      V(32)=V(22)
      V(27)=V(7)
      V(37)=V(17)
      N=4
      LV=1
      DO 99 L=1,N
      R(L)=V(LV)
      U(L)=V(LV+1)
      USER(10+L)=V(LV+2)
      USER(20+L)=V(LV+3)
      USER(30+L)=V(LV+4)
      USER(40+L)=V(LV+5)
      USER(50+L)=V(LV+6)
      USER(60+L)=V(LV+7)
      USER(70+L)=V(LV+8)
      USER(80+L)=V(LV+9)
   99 LV=LV+10
      ZERO=V(LV)
      RETURN
      END
      FUNCTION USERSF(FJ,BJ,SH,SK,IJ)
      COMMON/WORK/RA(200),DUMA(4640),U(200),NEXT(1600),V(100),IV(100),
     1X(100),Y(100),Z(100),NO(100),REST(3390),MOLFRA(4,10),SC(4),
     2Q(132),ZERO,ETA,CN(200),NSF,NDATA,USER(490)
      ANG=2.0*SK*(RA(IJ)-USER(30+IJ))+SH+BJ+USER(20+IJ)
      SKLIM=SQRT(2.0*(USER(50+IJ)-ZERO))/0.02916?
      IF(SK.LT.SKLIM)ANG=ANG+(SKLIM-SK)*USER(70+IJ)
      F=-FJ*USER(10+IJ)*SIN(ANG)
```

```
      IF(SK.LT.SKLIM)FJ=FJ*(1.0+(SKLIM-SK)*USER(70+IJ))
      F=-FJ*USER(10+IJ)*SIN(ARG)
```



```
      IF(SK.LT.SKLIM)F=F*(1.0+(SKLIM-SK)*USER(70+IJ))
      FP=2.0*PL(IJ)*USER(50+IJ)/(SK**USER(40+IJ))
      F=F*EXP(-2.0*S(IJ)*S(IJ)*SK*SK-FP)
      USERSF=F/(SK*RA(IJ)**2)
      RETURN
      END
####S
LIBRARY(DEPEND,NEW)
REWIND(LSD)
ADD(*,LSD)
FINISH.
####S
??INRAND(IN1=A,IN2=A)
??INRAND(IN1=A,IN2=A)
??INRAND(IN1=A,IN2=A)
??INRAND(IN1=A,IN2=A)
??INRAND(IN1=A,IN2=A)
??INRAND(IN1=A,IN2=A)
??INRAND(IN1=A,IN2=A)
??INRAND(IN1=A,IN2=A)
??INRAND(IN1=A,IN2=A)
??INRAND(IN1=A,IN2=A)
??INRAND(IN1=A,IN2=A)
??INRAND(IN1=A,IN2=A)
??INRAND(IN1=A,IN2=A)
??INRAND(IN1=A,IN2=A)
??INRAND(IN1=A,IN2=A)
??INRAND(IN2=CP)
  22   2   2                          R                    1   3(3F10.5)
   0.25565   0.02500  11.95055
??EXAFSLS1(OUTS=LP)
    MNSO4.(N-4)LSO4.SH2O
V/  1    2.150   0 R1?
V/  2    0.111   0 S1
V/  3    5.000   0 MULT R1
V/  4    0.000   0 PHASE R1
V/  5    1.500   0 FP R1?
V/  6    1.000   0 F-P POWER R1
V/  7    0.326   0 DELR1
V/  8    2.154   0 LIMIT
V/  9    0.000   0 UNUSED
V/ 10    0.000   0 UNUSED
V/ 11    4.320   0 R2
V/ 12    0.149   0 S2
V/ 13    7.271   0 MULT R2?
V/ 14    0.300   0 PHASE R2
V/ 15    1.500   0 F-P R2
V/ 16    1.000   0 F-P POWER R2
V/ 17    0.400   0 DELR2
V/ 18    0.000   0 UNUSED
V/ 19    0.000   0 UNUSED
V/ 20    0.000   0 UNUSED
V/ 21    3.550   0 R3?
V/ 22    0.167   0 S3
V/ 23    0.000   0 MULT R3
V/ 24    0.000   0 PHASE R3
V/ 25    1.000   0 FP R3?
V/ 26    1.000   0 F-P POWER R3
```

```
V/ 27   0.400  0 DELR3
V/ 28   0.000  0 UNUSED
V/ 29   0.000  0 UNUSED
V/ 30   0.000  0 UNUSED
V/ 31   4.000  0 R4
V/ 32   0.100  0 U4
V/ 33   0.000  0 MULT R4
V/ 34   0.000  0 PHASE R4
V/ 35   1.500  0 FP R4
V/ 36   1.000  0 FP POWER R4
V/ 37   0.400  0 DELR4
V/ 38   0.000  0 UNUSED
V/ 39   0.000  0 UNUSED
V/ 40   0.000  0 UNUSED
V/ 41   0.126  0 ZERO
R/  1  1  1  1  8
R/  2  1  1  1  8
R/  3  1  1  1  8
R/  4  1  1  1  8
SFDELK=  1 X 25,  1 X  7,  1 X  8,  1 X  1,  1 X 15
DATA/E= 1
TSAVER= 1
SHIFTX=0.01
CYCLES= 1
SCALES= 1.00    1
RADIAL DISTRIBUTION/M=  3,N=  3,DELR=0.050,RMAX= 6.00,CONST=0.010
LS END
??EXAFSCONT(LPPLOT,OUT3=LP)
UPHSCL=1.0
BCKGND/          0.90   11.95       1/USE CURVE 1 IN RAND
FTCORR=          1.0     1.0
??EXAFSLSQ(OUT3=LP)
SHIFTX=0.2
TSAVER= 0
CYCLES=20
SCALES= 1.00    0
V/  2   0.111  0 U1=U2
V/  7   0.326  0 DELR1
V/  8   2.154  0 LIMIT
V/  9   1.212  1 PH. ADJ. R1
V/ 10   2.394  1 AMP. ADJ R1
V/ 41   0.126  0 ZERO
??EXAFSCONT(LPPLOT,OUT3=LP)
FTCORR=3.0      1.0      1.0
BCKGND/          0.90   11.95       2/USE CURVE 1 IN RAND
??EXAFSLSQ(OUT3=LP)
TSAVER= 0
SCALES= 1.00    0
V/  8   2.154  1 LIMIT
V/ 41   0.126  0 ZERO
??EXAFSCONT(LPPLOT,OUT3=LP)
FTCORR=3.0      1.0      1.0
??END.
####S
```